Recent Winter Precipitation Increase in the Middle–Lower Yangtze River Valley since the Late 1970s: A Response to Warming in the Tropical Indian Ocean

XIAO-FENG LI

State Key Laboratory of Numerical Modeling for Atmospheric Sciences and Geophysical Fluid Dynamics, Institute of Atmospheric Physics, Chinese Academy of Sciences, Beijing, China

JIANPING LI

College of Global Change and Earth System Science, Beijing Normal University, Beijing, China

YUN LI

Data Analytics, CSIRO Digital Productivity Flagship, Floreat, Western Australia, Australia

(Manuscript received 14 October 2014, in final form 29 December 2014)

ABSTRACT

The middle–lower valley of the Yangtze River (MLY), located in the middle of eastern China, has been one of the largest economic centers of China since ancient times. Winter precipitation variability over the MLY is important for China because of its significant influence on the local economy. However, few studies have focused on the long-term variability of winter precipitation over the MLY. This study reports a significant wetting trend over the MLY in winter during the three decades since the late 1970s, forming a ''mid-east-China winter wetting'' pattern, which has become an important feature of precipitation change under the weakening East Asian winter monsoon. This wetting trend in the MLY also implies the poleward extension of the precipitation belts of southern China.

Further investigation reveals that the increasing sea surface temperature (SST) in the tropical Indian Ocean (TIO) is the dominant factor responsible for recent increases in precipitation over the MLY. The thermal forcing driven by warming of the TIO SST gives rise to an anomalous cyclonic circulation along the coast of eastern China. This transports more water vapor onto the Chinese mainland, shifts and causes anomalous convergence over the MLY, and generates the increase in precipitation there. As such, the increasing SST in the TIO induces over 80% of the observed wetting trend over the MLY. This mechanism was verified by results obtained from two sets of sensitivity experiments using a numerical spectral atmospheric general circulation model. Thus, increasing SST in the TIO has made a dominant contribution to the recent winter precipitation increase over the MLY.

1. Introduction

The middle–lower Yangtze River (or Changjiang River) valley (MLY) is one of China's largest economic centers. It is located in the middle of eastern China, and has been known as ''the land of fish and rice'' since ancient times. Changes in winter [December–February (DJF)] precipitation (rain and snow) are vital to this area because of the associated significant impacts on local agricultural and industrial productivity, water supply, transportation, energy consumption, ecological equilibrium, and other factors. For instance, the anomalously heavy snow and rainfall that hit the MLY and other parts of middle and southern China during the winter of 2008 (e.g., W. Zhou et al. 2009; Zhou et al. 2011) seriously disrupted local electricity supply and transportation, causing damages estimated to be worth more than 1 billion U.S. dollars and affecting more than 100 million people (e.g., Zhou et al. 2011). The above influences of the positive MLY precipitation event on the local economy

Denotes Open Access content.

Corresponding author address: Prof. Jianping Li, College of Global Change and Earth System Science, Beijing Normal University, No. 19, XinJieKouWai St., Haidian District, Beijing 100875, China.
E-mail: ljp@bnu.edu.cn

DOI: 10.1175/JCLI-D-14-00701.1

is a warning to us that the long-term precipitation increase in MLY could cause more disasters in MLY area. Therefore, it is necessary to pay more attention to the long-term winter precipitation changes over the MLY.

Various efforts have been made to develop a better understanding of the variability associated with the trend in winter precipitation across China. A few studies have focused on southern China because most winter precipitation in China falls in this region (e.g., Zhou and Wu 2010; Zhang et al. 2011), and the biggest interannual variance of winter precipitation in China also occurs in this region (e.g., Wang and Feng 2011). It is reported (e.g., Gemmer et al. 2004; Zhai et al. 2005; Liao et al. 2013) that the winter precipitation has significantly increased in small parts of southern China and Tibet during the second half of the twentieth century. This precipitation increase in southern China has been attributed to both a stronger Arctic Oscillation (AO) (e.g., Shuai et al. 2010; Zhang et al. 2014) and a warmer western Pacific surface (e.g., Zhang et al. 2014). A stronger positive AO weakens the southward polar flow that brings less dry and cold air mass to southern China from high latitudes, and a warmer western Pacific Ocean enhances the anomalous anticyclone over Japan that brings more moisture to southern China from neighboring oceans, resulting in more precipitation over southern China (e.g., Shuai et al. 2010; Zhang et al. 2014). In contrast, little research has focused on the long-term variability in wintertime precipitation over the MLY, although the MLY is an important economic center of China that can be heavily influenced by long-term precipitation variability. This is mainly as a result of the limited datasets available to the early studies (e.g., Zhai and Pan 2003), which found no evident trend in winter precipitation over the MLY during the second half of the twentieth century. With the accumulation of the longer high-quality datasets, we try to explore the long-term variability in winter precipitation over the MLY again in this study.

On the other hand, it is well known that the global climate system has experienced a unique period in the three decades since the late 1970s (the middle of the second half of twentieth century). During this period, the global climate system has not only had its warmest three decades in the most recent century (IPCC 2013), but has also abruptly shifted to a new regime (e.g., Nitta and Yamada 1989; Trenberth 1990; Trenberth and Hurrell 1994; Mantua et al. 1997; Zhang et al. 1997b). This regime shift under a warming scenario was marked by a series of abrupt decadal changes that occurred in the atmospheric and oceanic system around 1976 (e.g., Nitta and Yamada 1989; Trenberth 1990; Trenberth and Hurrell 1994; Mantua et al. 1997; Zhang et al. 1997), which influenced regional precipitation changes globally, including in China. For example, the DJF rainfall trend over northern Australia changed from a dipole pattern (east dry and west wet) to a uniform wetting trend after the late 1970s (Li et al. 2013); rainfall characteristics in India (Kumar et al. 1999) and Korea (Ho et al. 2003) also shifted between ''dry'' and ''wet'' conditions around this period; and the summer rainfall over the MLY and the whole of eastern China experienced a notable regime shift after 1979 (Gong and Ho 2002). Therefore, the following question arises: Did precipitation variability over the MLY in winter still show no significant trend during this warming period under the new climate regime since the late 1970s?

Given that the recent decadal shift in the global atmospheric and oceanic system occurred around 1976 (e.g., Nitta and Yamada 1989; Trenberth 1990; Trenberth and Hurrell 1994; Mantua et al. 1997; Zhang et al. 1997), we therefore reexamine the wintertime precipitation trend over the MLY in the post-1976 period using the newest station and gridded datasets and then illuminate the dynamic mechanism driving the trend variability in MLY precipitation. The remainder of this paper is organized as follows. Section 2 presents data, methods, and a brief introduction to the numerical spectral atmospheric general circulation model (AGCM) used in this study. In section 3, we present the observed precipitation trends over the MLY for the winters of 1976–2009. In sections 4 to 6, we explore the driving factors of the MLY precipitation trend, propose a physical mechanism, and then test and improve the mechanism using two sets of sensitive experiments of the AGCM. Finally, the discussion and summary are presented in section 7.

2. Data and methods

a. Data

The rainfall data analyzed here were provided by the National Meteorological Information Center (NMIC) of the China Meteorological Administration (CMA) and consist of both the gridded reanalysis and station observational data. The spatial resolution of the gridded rainfall is $0.25° \times 0.25°$, which was interpolated from daily observations of over 2400 national meteorological stations in China (Shen et al. 2010). The station rainfall data were observed by 194 international exchange stations across China (a subset of the entire Chinese network). Stations with missing values in winter or with a location that had been shifted during the study period were excluded, and this left a total of 174 stations from which data were obtained. Both of the above rainfall datasets are for winters in the period of 1976–2009.

The intensity indices of the well-known active teleconnection patterns in the winter season in the extratropics of the Northern Hemisphere were used in this study, including the conventional Eurasian (EU) pattern, the east Atlantic–western Russia pattern (EATL/WRUS), the Scandinavia pattern (SCAND), the North Atlantic Oscillation (NAO), the east Atlantic pattern (EA), the Polar–Eurasia pattern (POL), the west Pacific pattern (WP), the east Pacific–North Pacific pattern (EP–NP), the Pacific–North American pattern (PNA), and the tropical–Northern Hemisphere pattern (TNH). The above indices were downloaded from the website of the National Oceanic and Atmospheric Administration (NOAA) Climate Prediction Center (CPC) (http://www.cpc.ncep.noaa.gov/data/teledoc/teleintro.shtml), except for the EU, EATL/WRUS, and SCAND indices. The intensity indices of the later three teleconnection patterns were taken from Liu et al. (2014). It should be noted that the selection of teleconnection pattern indices does not change the main results in this study.

The SST data used were from the improved NOAA Extended Reconstructed SST, version 3b (ERSST.v3b), dataset (Smith et al. 2008), with a resolution of $2° \times 2°$ gridded points and downloaded from the NOAA website (http://www.ncdc.noaa.gov/ersst/). Monthly gridded data for wind and sea level pressure (SLP), skin temperature (SKT), total cloud cover (TCDC), and other commonly used climate variables were obtained from the NCEP-1 reanalysis data. All data covered the period from January 1976 to February 2010, and the anomalies were calculated relative to the climatology for the period 1971–2000.

b. Methods

Linear regression was used to estimate the linear trend in both observed precipitation and specific climate modes [e.g., tropical Indian Ocean (TIO)]. The regression coefficient or slope was used to represent the linear trend. Correlation and partial correlation were also employed to estimate the influence of a specific climate mode on the MLY wetting trend.

The contribution of a specific climate mode (e.g., TIO) to the wetting trend of the MLY was determined using the methods of Nicholls (2010) and Li et al. (2013). We calculated the partial correlations between rainfall and year of observation by removing the influence of the index of a specific climate mode (e.g., TIO). The correlation value between rainfall and the year of observation indicates the significance of the linear trend in rainfall. If the partial correlations, after removing the variations in the specific climate mode, are close to zero, then much of the rainfall trend is related to the trend in that climate mode; otherwise, the rainfall trend is unlikely to be controlled by that climate mode.

To further quantify the contribution of a specific climate mode (e.g., TIO) to the MLY precipitation wetting trend, the year-to-year differences (also known as first-order differences) of MLY precipitation were regressed onto those of the climate mode index. The slope of this regression was defined as the sensitivity of precipitation to the climate mode, which represents the response of MLY precipitation (in millimeters) to one unit variation of the climate mode index over interannual time scales. Assuming that the relationship derived from the year-to-year values also operates over multidecadal time scales, this sensitivity can then be used to estimate the MLY precipitation increase that could be associated with the observed trend in the climate mode (Nicholls 2010; Li et al. 2013). This approach removes the possibility that any relationship between the climate mode index and the rainfall is simply due to trends in the variables rather than reflecting a relationship that is valid across all climatic time scales (Nicholls 2010).

c. Model description

We used a numerical model to verify whether the winter MLY precipitation trend is driven by changes in SST: the spectral AGCM developed at the State Key Laboratory of Numerical Modeling for Atmospheric Sciences and Geophysical Fluid Dynamics (LASG), Institute of Atmospheric Physics (IAP), Chinese Academy of Sciences (CAS), Beijing, China. This model has nine vertical levels and is rhomboidally truncated at wavenumber 42 in the horizontal [i.e., the Global Ocean–Atmosphere–Land System (GOALS) Spectral Atmospheric Model version R42L9 (SAMIL-R42L9); Wu et al. 1997; Wu et al. 2003; Wu et al. 2007]. The early version of this model was designed by Bourke (1974) and further developed by Simmonds (1985). This numerical model can accurately simulate the main characteristics of the observed climatology in MLY and other East Asia areas, including SLP, precipitation, specific humidity, geopotential height, temperature, and winds (Wu et al. 2003; Wu et al. 2012).

3. Observed wetting trend over the MLY since 1976

Indeed, the winter precipitation variability over MLY is significantly tending up in the post-1976 period (Fig. 1). Figure 1 shows the linear trend of DJF total precipitation (rain and snow) over mainland China for the period 1976–2009. A dominant increasing trend in precipitation is evident for the MLY in both the gridded reanalysis data (Fig. 1a) and the observational data from the stations (Fig. 1b). The significant increasing trends in gridded data

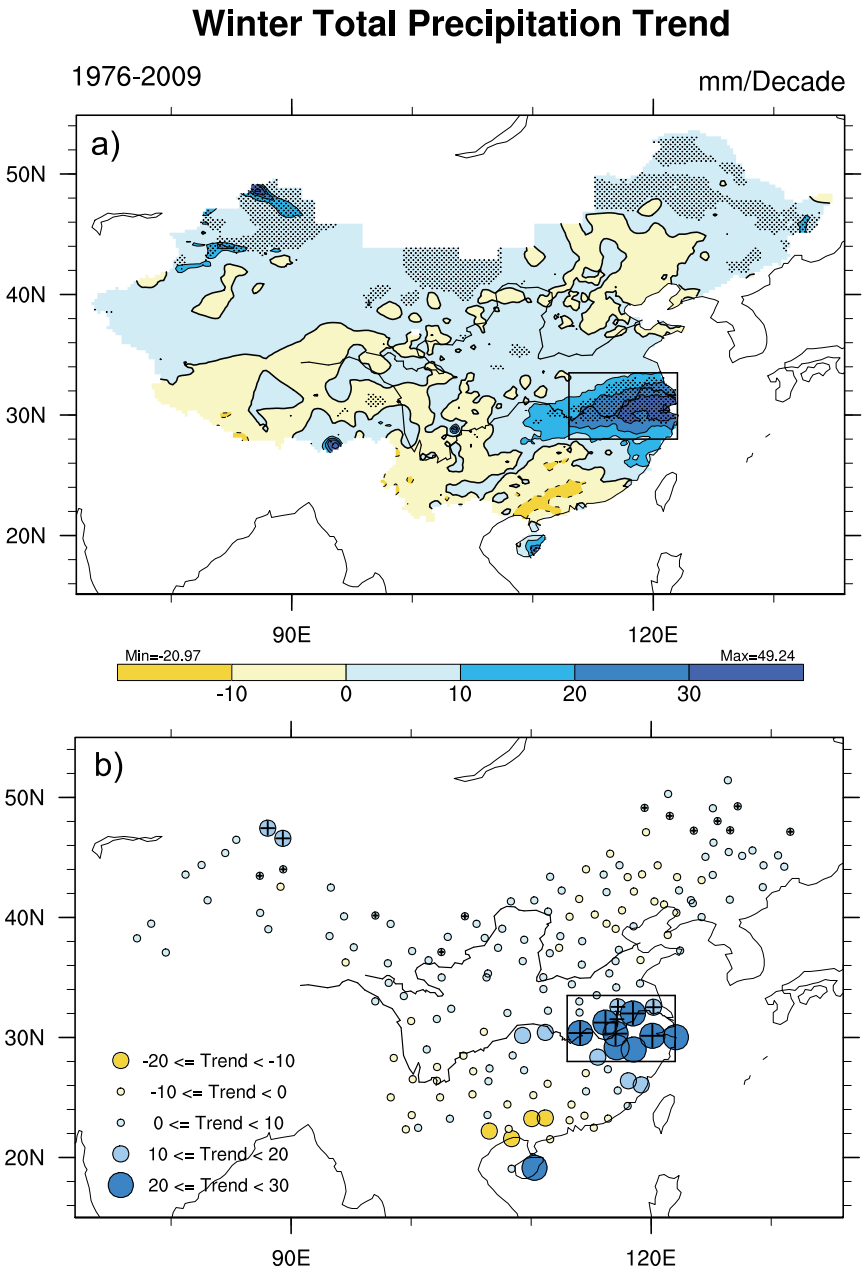

FIG. 1. Spatial pattern of winter (DJF) total precipitation trend (mm decade^{-1}) over the 34 yr from 1976 to 2009 based on (a) the NMIC/CMA gridded rainfall data and (b) station rainfall data. The contour interval in (a) is 10; thin black (thin dashed) contours denote positive (negative) trends; the bold black contours denote zero. Trends significant at the 0.05 level are indicated by black dots in (a) and by stations marked by the + symbol in (b). The effective sample sizes (not shown) were reestimated (Bartlett 1935; Zwiers and von Storch 1995) to test the significance of the trend. The black rectangle marks the MLY area (28°–33.5°N, 113°–122°E), and the average winter total precipitation in this area in (a) is defined as the MLYP.

are mainly located in the lower valley of the Yangtze River and extend upstream to its middle valley, with the maximum positive trend exceeding 49 mm decade^{-1}. The significant increase of winter precipitation in the MLY is also clearly recorded in individual instrumental records. As shown in Fig. 1b, the trend of increasing precipitation is evident for most stations across the MLY. The averaged gridded precipitation over the MLY within the area 28°–33.5°N, 113°–133°E (marked by the box in Fig. 1) was used to represent the MLY precipitation (MLYP)

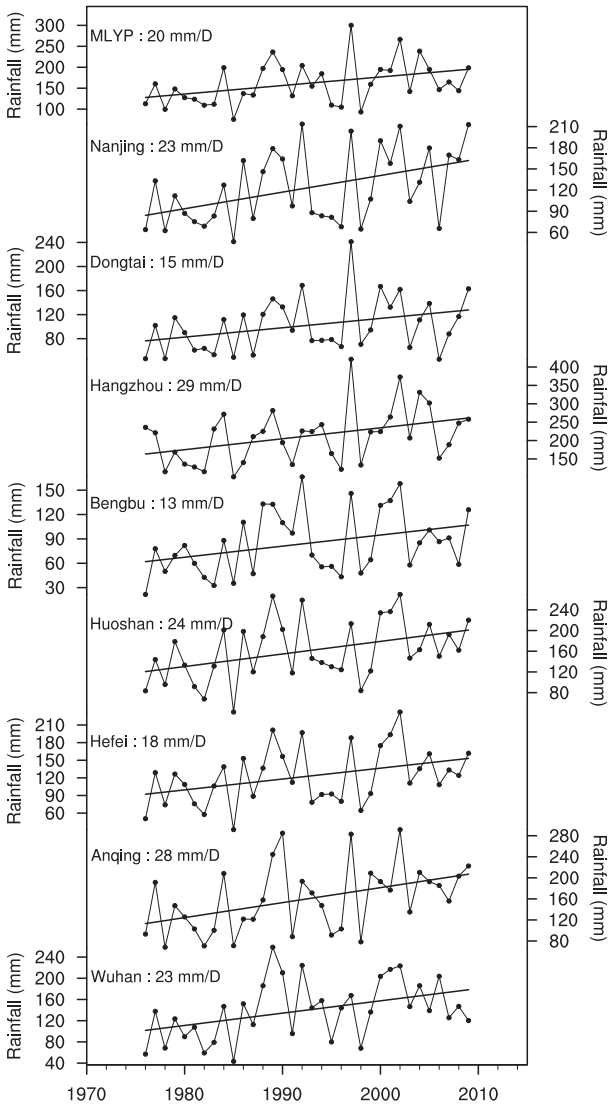

FIG. 2. Time series (curves with dots) and linear trends (straight lines) of the winter total precipitation at (top to bottom) nine selected high-quality stations in MLY. All the time series contain statistically significant (at the 0.05 level) positive trends (indicated on each panel). The effective sample sizes (not shown) were re-estimated (Bartlett 1935; Zwiers and von Storch 1995) to test the significance of the trend.

variability (Fig. 2). The MLYP represents the MLY precipitation variability very well, as demonstrated by its significant correlations with the precipitation centering in the MLY area (Fig. 3). And its time series shows a positive trend with a slope of 20 mm decade^{-1} (Fig. 2), which is significant at the 0.05 level. In particular, the precipitation series of 8 stations (out of 13) show increasing trends, significant at the 0.05 level (Figs. 1b and 2). Among them, the two stations that have the strongest wetting trend are located at Hangzhou and Anqing, where the recorded increase was 29 and 28 mm decade^{-1}, respectively. Thus, a positive precipitation trend has dominated the MLY over the past 34 winters, since the late 1970s.

As the MLY is located in the middle part of eastern China, the significant precipitation increase over the MLY in winter is also called a "mid-east-China winter wetting" in this study. This mid-east-China winter wetting pattern since the late 1970s (1976–2009) differs significantly from the precipitation trend previously observed during the second half of the twentieth century (1951–2000). As documented by Zhai et al. (2005), wintertime precipitation increased significantly over Tibet and small areas of southern China, but there was a significant decrease over most parts of northeast, north, and eastern-northwest China, as well as the Sichuan basin, during the period 1951–2000. In particular, no significant trends were observed over the MLY during this period (e.g., compare our Fig. 1 with Fig. 3b in Zhai et al. 2005). Therefore, dramatic changes have occurred in winter precipitation over China since the late 1970s.

4. East Asian winter monsoon and MLY wetting

The East Asian winter monsoon (EAWM) prevails over China in the winter and strongly modulates the local climate (e.g., Zhang et al. 1997; Nakamura et al. 2002; Chang 2004), occasionally with disastrous results (e.g., Huang et al. 2007; Wu et al. 2011; Zhou et al. 2011). The question to be addressed in this section is: What is the connection between the MLY wetting and the EAWM? The EAWM is known to be a very complex climate system, which is hard to describe perfectly with one specific index. More than 18 EAWM indices have been proposed, which perform well at catching different aspects of the EAWM's variability (Wang and Chen 2010). And new EAWM indices are continuously coming out to complement them (Wang and Chen 2014). So, we investigate the connection between the MLY wetting and the EAWM directly from the circulations to get a more general view.

Figure 4a shows that the correlation between the MLYP and horizontal wind vectors at 850 hPa manifests itself in cyclonic southerlies along the coastal area of eastern China. This suggests that a stronger cyclonic southerly brings more precipitation to the MLY area. In particular, the southwesterly prevails in the southern MLY and the southeasterly prevails in the northern MLY, which causes anomalous convergence and increased cloudiness (Fig. 4b) over the MLY and, consequently, more precipitation. As the prevailing anticyclonic northerly wind (cold and dry) along eastern China (as shown in Fig. 5a) is one of the prominent features of the EAWM (e.g., Chang et al. 1979; Ding and Krishnamurti 1987; Zhang et al. 1997),

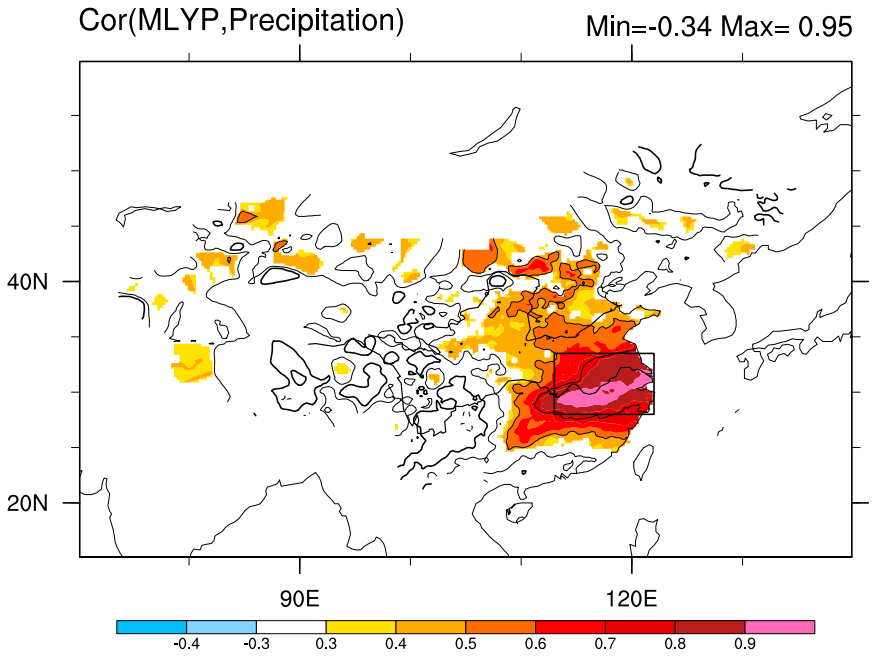

FIG. 3. Correlation of the MLYP with precipitation over China in winter during the period 1976–2009. The contour interval is 0.25; thin black (thin dashed) contours denote positive (negative) trends; the bold black contours denote zero. The areas significant at the 0.05 level are colored. The effective degrees of freedom were estimated according to Pyper and Peterman (1998).

we can infer that an increase in precipitation over the MLY usually occurs against the background of a weaker EAWM circulation over the coast of eastern China, and vice versa. Consequently, MLYP variability is closely connected to the EAWM circulation. And this negative connection between MLYP and EAWM is consistent with previous studies (e.g., Zhou 2011).

Moreover, the EAWM circulation is weakening during the winters of 1976–2009. As mentioned above, the EAWM circulation can be represented by the reversal or difference of horizontal circulations between the winter and summer season, which manifests as the anticyclonic northerlies along eastern China in the troposphere (Fig. 5a). In contrast, the linear trend of the horizontal winds (Fig. 5b) is opposite to the EAWM circulation, which exhibits as the cyclonic southerlies along the coastal area of eastern China, indicating the EAWM circulation in this area is weakening during the period of 1976–2009. Actually, Xu et al. (2006) has already observed that winter wind speeds over East Asia (mainly the northerly wind) have been declining steadily, and subsequent studies (e.g., Wang et al. 2009; Hung and Kao 2010; Wang and Chen 2010) have verified their results, which all support a weakening EAWM in recent decades. Given that more precipitation over the MLY usually occurs against the background of a weaker EAWM circulation (as demonstrated above), it seems reasonable to suggest that a weakening EAWM causes a wetting MLY in recent decades. Therefore, we conclude that the wetting trend over the MLY can be generally attributed to the weakening of the EAWM.

Here, we also report that the wetting trend in the MLY or the mid-east-China winter wetting in the period of 1976–2009 is an important feature of the regional climate change under the weakening EAWM in recent decades. This mid-east-China winter wetting pattern could be either an indicator for the examination of the performance of existing EAWM indices or a reference for the definition of a new EAWM index in the future.

5. Remote causes of MLY wetting

As mentioned above, the wetting trend over the MLY can be generally attributed to the weakening of the EAWM system. However, the EAWM is a local circulation system (prevailing over East Asia), and its interannual, decadal, and longer-term variabilities are modulated heavily by remote factors, such as SST (e.g., Zhang et al. 1997), sea ice (e.g., Li and Wu 2012), wave activity (e.g., Chen et al. 2005), and remote advection (e.g., Wu et al. 2009; Lee et al. 2013). This motivates us further to explore the ultimate remote causes responsible for this recent MLY wetting by modulating the local circulations over MLY (e.g., EAWM). And we investigated the potential drivers from both the high latitudes and the tropics. To this end, there are two

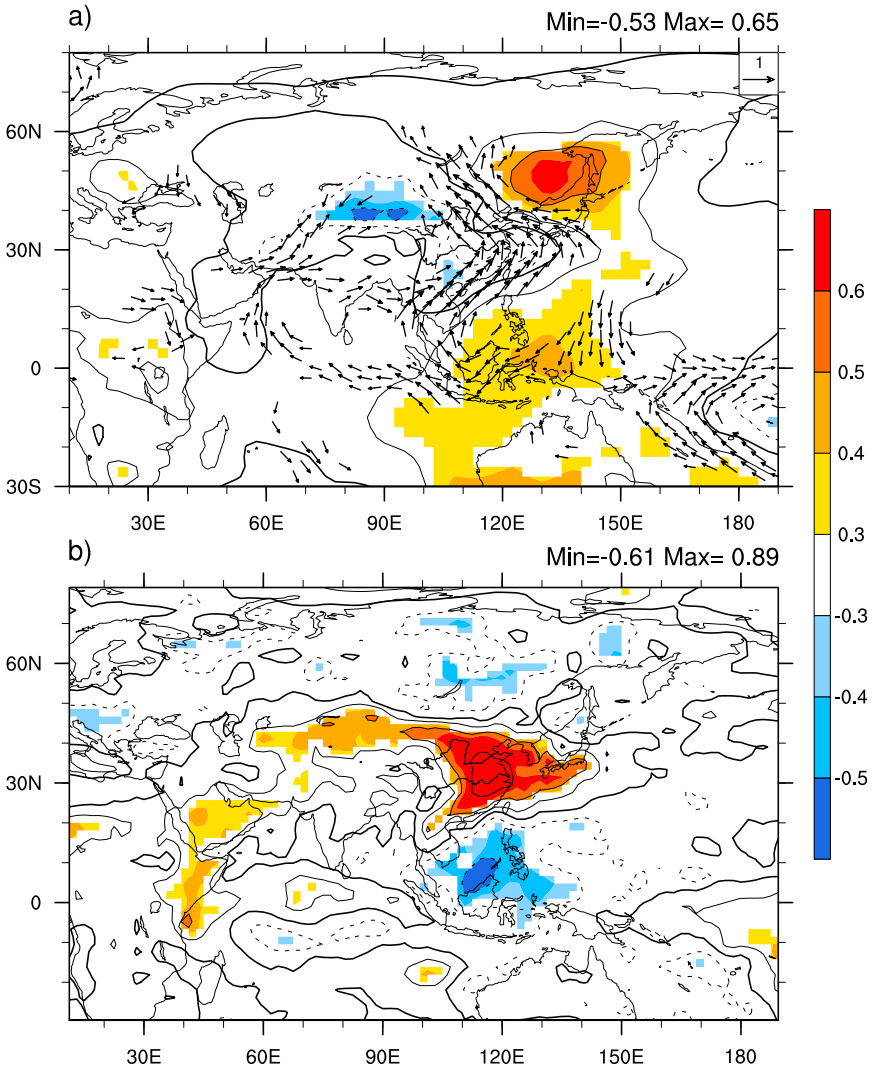

FIG. 4. Correlation of the MLYP with (a) SLP (contours) and horizontal wind (vectors) at 850 hPa, (b) TCDC (contours) in winter during the period 1976–2009. The vectors are of correlations significant above the 0.10 level for which the two components are the correlation coefficients between the MLYP and anomalously zonal wind, and between the MLYP and anomalously meridional wind velocity. The contour interval is 0.25; thin black (thin dashed) contours denote positive (negative) trends; the bold black contours denote zero. The areas significant at the 0.10 level are colored, and the minimum and maximum values of contours are denoted on the left top of each panel. The effective degrees of freedom were estimated according to Pyper and Peterman (1998).

independent factors—a wave train teleconnection pattern extending from European high latitudes and SST in the tropical Indian Ocean—drawing our attention because of their significant correlations with the MLYP variability.

a. Connection between the EATL/WRUS pattern and MLY wetting

In Fig. 6, a wave train structure or pattern is observed in correlation maps between the MLYP and geopotential height (HGT). This wave train pattern emerges as the '+−+' significant correlation between the MLYP and HGT, which started in Europe and then extended downstream to western Russia before reaching northeast China. This wave train pattern can be observed in both the troposphere and lower stratosphere, including the isobaric surfaces at 850 (Fig. 6a), 500 (Fig. 6b), and 300 hPa (Fig. 6c), indicating its quasi-barotropic nature at mid–high latitudes. In particular, the maximum correlations between the MLYP and HGT occur over western Russia and northwest China on the 850-hPa isobaric surface, suggesting the wave train pattern influences the MLYP mainly through its last two centers in

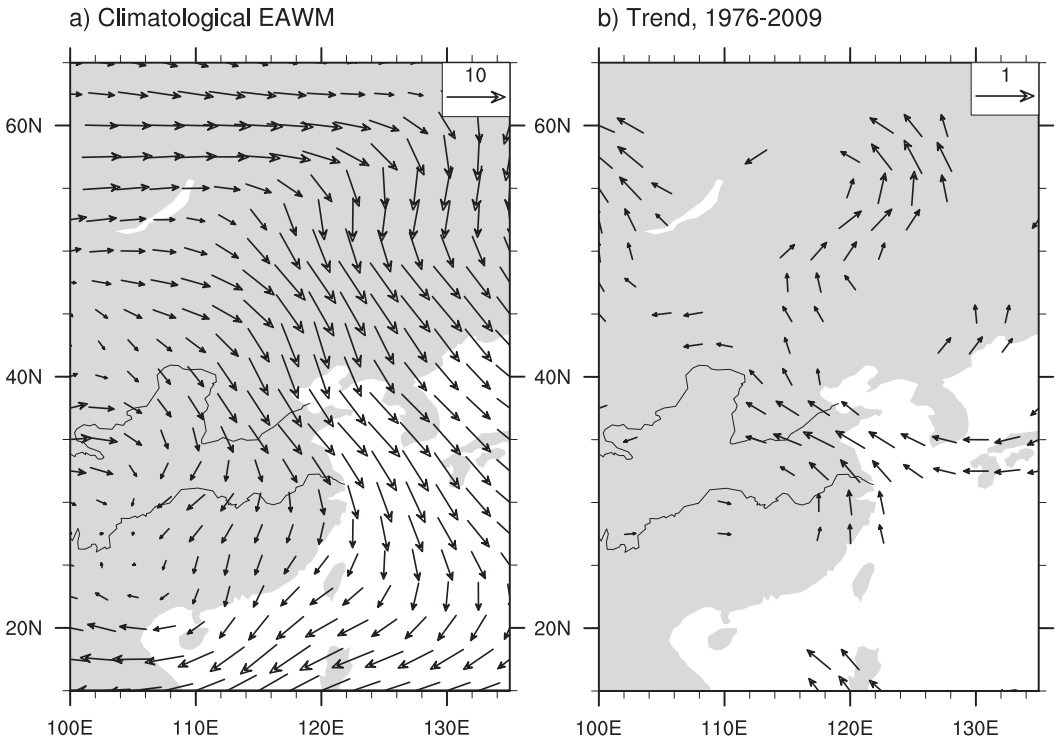

FIG. 5. Maps of (a) the climatological EAWM circulations represented by the difference of the horizontal circulations ($m\,s^{-1}$) in winter to that in summer at 850 hPa during the period 1951–2000 and (b) the linear trends of horizontal wind (vectors) at 850 hPa in winter during the period 1976–2009. The vectors in (b) are of linear trends significant above the 0.05 level for which the two components are the slopes of zonal and meridional wind ($m\,s^{-1}$ decade^{-1}). The effective sample sizes (not shown) were reestimated (Bartlett 1935; Zwiers and von Storch 1995) to test the significance of the trend.

the lower troposphere. As shown in Fig. 4a, the last two centers of the intensified wave train are located over northern China, which causes the wind to shift from an anomalous southwest wind to a southeast wind over the MLY and induces anomalous convergence over the MLY, resulting in a wetter MLY, and vice versa. Therefore, the wave train structure extending downstream from Europe and west Russia strongly modulates the MLYP variability.

There are many different kinds of teleconnection wave train patterns active in the mid–high latitudes of the Northern Hemisphere in winter (e.g., Wallace and Gutzler 1981), but what is the wave train pattern observed in this study (Fig. 4)? To identify this, we calculated the temporal correlations between the time series of MLYP and the well-known active teleconnection patterns in the winter season of the extratropics of the Northern Hemisphere, including the EU, EATL/WRUS, SCAND, NAO, EA, POL, WP, EP–NP, PNA, and TNH [see Liu et al. (2014) and http://www.cpc.ncep.noaa.gov/data/teledoc/teleintro.shtml]. As shown in Table 1, only the correlation coefficient between the time series of MLYP and the EATL/WRUS pattern reaches 0.34, significant at the 0.05 level after re-estimating the efficient number of degrees of freedom (Pyper and Peterman 1998; Li et al. 2012). This indicates that a stronger (weaker) EATL/WRUS pattern is associated with more (less) precipitation over the MLYP, and other active teleconnection patterns examined in Table 1 may have less influence on MLYP during the same period. Consequently, we conducted spatial correlations between the spatial pattern (correlation pattern between intensity index and geopotential height field) of EATL/WRUS and the wave train pattern related to MLYP variability (Fig. 4) in the extratropics in the Northern Hemisphere. We confirmed that the wave train related to MLYP variability shown in Fig. 4 is very similar to the EATL/WRUS pattern, which is one of the types of Eurasian pattern (Barnston and Livezey 1987; Liu et al. 2014). The spatial correlation between the EATL/WRUS pattern and the wave train pattern related to MLYP (Fig. 4) in mid–high latitudes north of 20°N reaches 0.66, 0.67, and 0.62 on the 850-, 500-, and 300-hPa isobaric surfaces, respectively, all significant at the 0.05 level. Therefore, the wave train structure in the correlation map in Fig. 4 implies that the EATL/WRUS pattern modulates the MLYP variability from mid–high

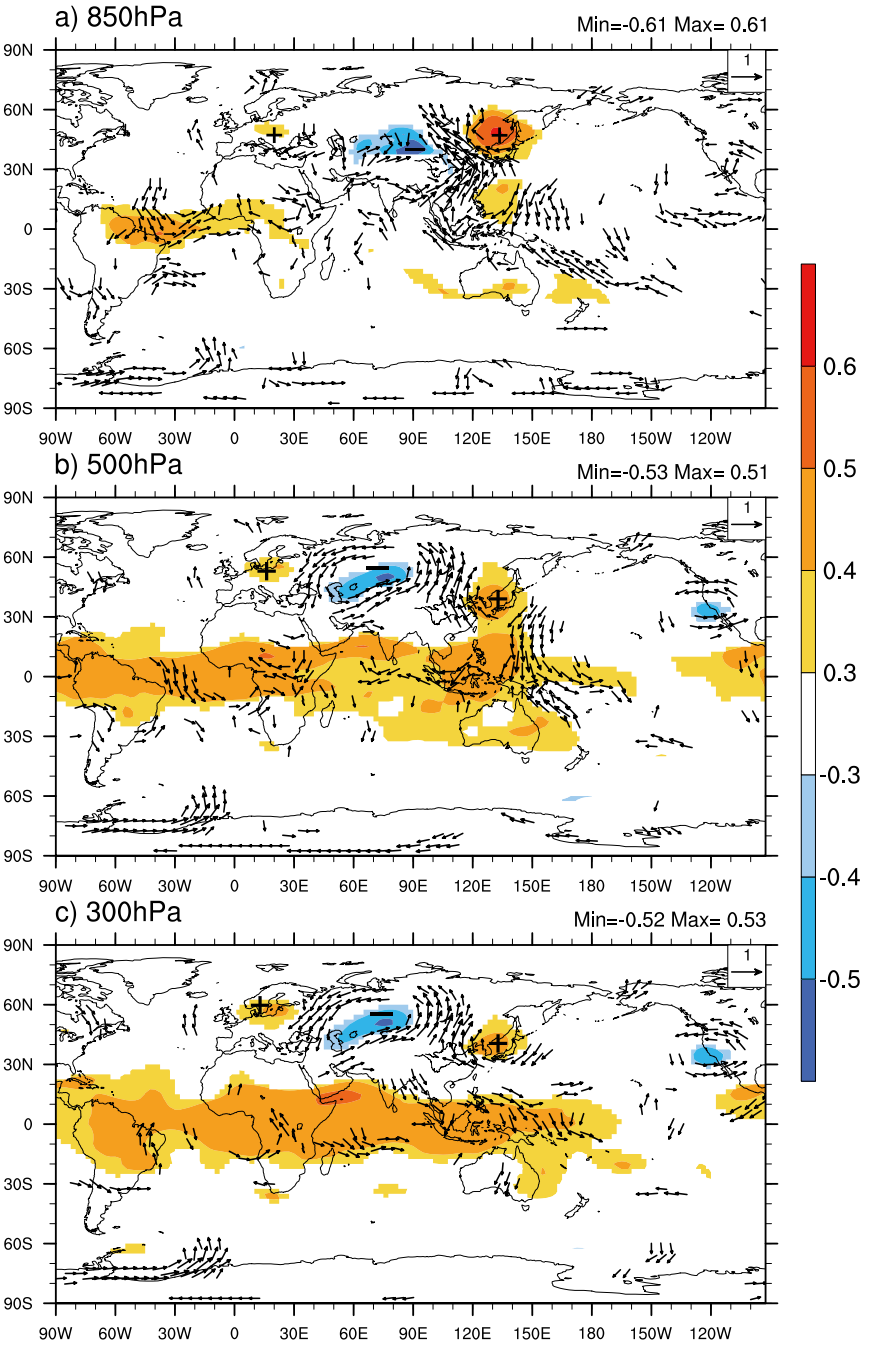

FIG. 6. Maps showing the correlation between the MLYP and HGT (color shading) and horizontal wind (vectors) at (a) 850, (b) 500, and (c) 300 hPa in winter during the period 1976–2009. The vector here is of correlations significant above the 0.10 level for which the two components are the correlation coefficients between the MLYP and anomalously zonal wind and between the MLYP and anomalously meridional wind velocity. The areas significant at the 0.10 level are colored. The effective degrees of freedom were estimated according to (Pyper and Peterman (1998)). The centers of the wave train teleconnection pattern in HGT filed are marked with + and − symbols.

TABLE 1. Correlations between the MLYP and teleconnection patterns in the extratropics of NH. Data are for winters from 1976 to 2009. The intensity indices of the teleconnection patterns are from the NOAA CPC (http://www.cpc.ncep.noaa.gov/data/teledoc/teleintro.shtml), except the conventional EU, EATL/WRUS, and SCAND indices, which are from Liu et al. (2014). Correlations significant at the 0.05 level are in bold. The effective degrees of freedom were estimated according to Pyper and Peterman (1998).

	EU	EATL/WRUS	SCAND	NAO	EA	POL	WP	EP–NP	PNA	TNH
MLYP	0.08	**0.34**	0.06	0.08	0.25	−0.05	0.20	−0.03	0.003	−0.04

latitudes. The above results are consistent with those of a previous study (Liu et al. 2014), which concluded that the EATL/WRUS pattern strongly influences wintertime precipitation over eastern China.

Wang and Feng (2011) has documented that the SCAND teleconnection pattern has an important influence on wintertime MLY precipitation variability using the station data in the period 1951–2009. We confirmed that the SCAND pattern is significantly correlated with MLYP in a longer time period, such as 1960–2009 (confined by our rainfall data length), which supports their results (Wang and Feng 2011). However, this significant correlation between SCAND pattern and MLYP drops to near zero (see Table 1) during the period of 1976–2009, indicating the weakened connection between the SCAND pattern and MLYP during our research period. Thus, the connection between the SCAND pattern and winter MLYP is unstable in different temporal periods, and it is very weak in recent decades, since the late 1970s.

Although the EATL/WRUS teleconnection pattern strongly modulates the MLYP variability through its last two action centers in the lower troposphere (Fig. 6), it contributes only a little to the recent linear trend of MLYP because it has shown no significant upward trend in recent decades. The correlation coefficient of the EATL/WRUS pattern index with the year is only 0.15 (Table 2), indicating no significant linear trends exists in the EATL/WRUS pattern in recent decades. Furthermore, an EATL/WRUS pattern with no upward trend is unlikely to cause a significant wetting trend over the MLY.

b. *Connection between Indian Ocean SST and MLY wetting*

Figure 7a shows the correlation between the MLYP and SST over the Indo-Pacific Ocean. There are significant positive correlations in the tropical Indian Ocean, indicating that an increase in MLY precipitation is associated with a warmer SST over the TIO in recent decades, and vice versa. To highlight the influence of the TIO, we defined the TIO index (TIOI) as the averaged SST over the rectangular box (13°S–20°N, 40°–125°E) and calculated the correlations between the TIOI and the precipitations over mainland China. It is found that the correlation coefficient between the time series of TIOI and MLYP is 0.54, significant at the 0.05 level (Table 2). Moreover, correlating the time series of TIOI with gridded precipitation over mainland China (Fig. 7b), we see a significant correlation pattern centered over the MLY in eastern China, suggesting that the precipitation pattern associated with the TIOI is similar to the recent precipitation trend (cf. Fig. 7b and Figs. 1a,b). In addition to the correlations, a singular value decomposition (SVD) analysis is also used to verify the relationship between the MLY precipitation and the Indo–Pacific Ocean SSTs (Fig. 8). The first SVD mode accounts for 30.7% of the total squared covariance. The winter precipitation pattern of the leading SVD is mainly characterized by the signature of precipitation with evident positive correlation over the MLY, and the winter SST pattern of the leading SVD shows a significant correlation over the TIO. This implies that the warmer TIO will be followed by a stronger DJF precipitation over the MLY. Therefore, both the correlations and the SVD analysis lead to the same conclusion: a warmer TIO is usually followed by a wetter MLY in winter, and vice versa.

The SST over the TIO is not only significantly correlated with MLY precipitation, but has also shown an upward trend in recent decades. As shown in Fig. 9, a general increase in warming SSTs has been observed in neighboring oceans around mainland China since the late 1970s. In particular, significant warming is observed in the TIO region, directly to the south of mainland China (Fig. 9). The TIOI has a strong correlation (0.55) with the year, which is significant at the 0.05 level (Table 2), demonstrating a significantly upward trend in recent decades. The warming of the TIO has been documented in several previous

TABLE 2. Correlations among MLYP, year, EATL/WRUS pattern index, and TIOI. Data are for winters from 1976 to 2009. Correlations are for each variable with year and partial correlations between rainfall and year, after the removal of signals of the variable at the head of each column. Correlations significant at the 0.05 level are in bold. The effective sample sizes were reestimated according to Zwiers and von Storch (1995).

	EATL/WRUS pattern index	TIOI
Correlation with MLYP	**0.34**	**0.55**
Correlation with year	0.15	**0.60**
Partial correlation of MLYP with year (correlation of MLYP with year is **0.39**)	**0.36**	0.08

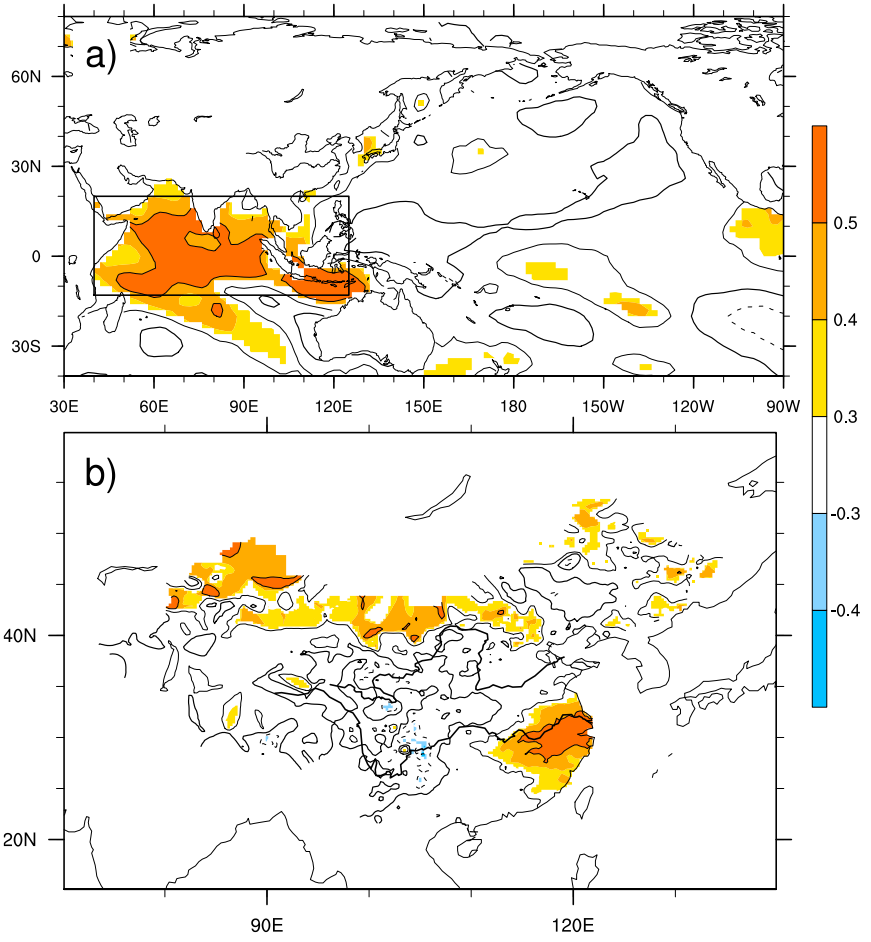

FIG. 7. Maps of correlations between (a) the MLYP with SST, and (b) the TIOI with precipitation over China in winter during the period 1976–2009. The contour interval is 0.25; thin black (thin dashed) contours denote positive (negative) trends; the bold black contours denote zero. The areas significant at the 0.10 level are colored. The effective degrees of freedom are estimated according to Pyper and Peterman (1998). Rectangular box in (a) marks the tropical TIO area (13°S–20°N, 40°–125°E); the average SST over this box is defined as the TIOI.

studies (e.g., Webster et al. 1999; Hoerling et al. 2001; Barnett et al. 2005; Levitus et al. 2005; Deser and Phillips 2006; Alory et al. 2007; Rao et al. 2012), and this supports the above observational results of the present study.

Given the significantly positive connection between TIOI and MLYP, a strong warming in the TIO may play an important role in causing the wetting trend over MLY. Now we focus on its influence on the recent increase in MLYP.

c. *Contributions of TIO warming to recent MLY wetting*

Following Nicholls (2010) and Li et al. (2013), a partial correlation method was used to investigate the contribution of increasing TIO SST to the wetting trend of MLY averaged winter precipitation. The correlation between MLYP and the year is 0.34 (Table 2), which is significant at the 0.05 level after taking account of autocorrelation in the data by using the trend analysis in Li et al. (2013). This result suggests a significant increasing trend in MLYP. After removing the linear influence of TIOI, the partial correlation between MLYP and the year drops to 0.08, which is not significant (Table 2), indicating that most of the increase in rainfall is associated with the warming trend in the TIO. In contrast, after removing the influence of the EATL/WRUS teleconnection pattern, the partial correlation between MLYP and the year did not decrease, but increased to 0.36, which is still significant at the 0.05 level (Table 2). This result further demonstrates that the increase in MLYP is mainly associated with, or induced by, the TIO but not the EATL/WRUS teleconnection pattern at mid–high latitudes.

To assess how much of the recent MLY wetting trend was caused by a warming SST in the TIO, year-to-year

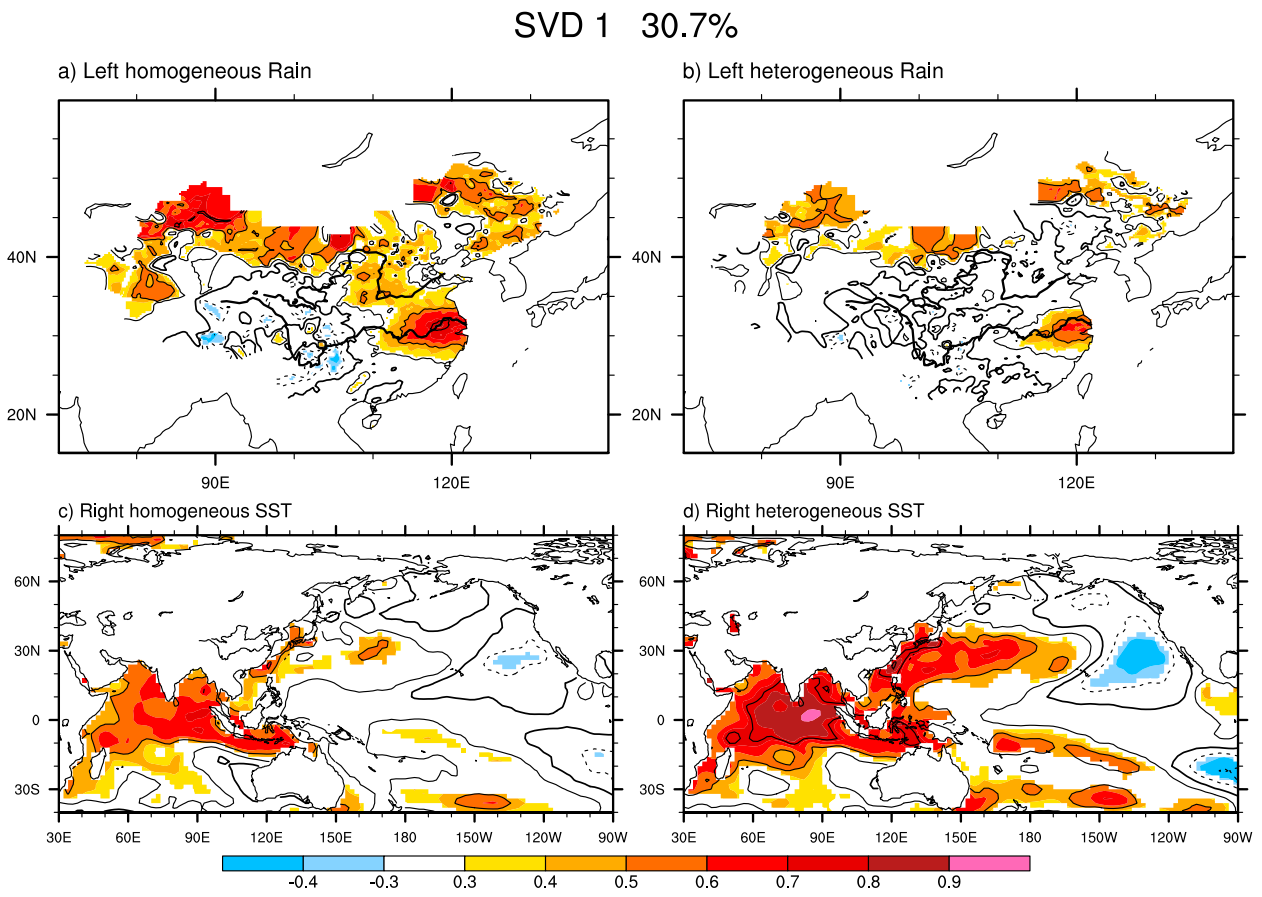

FIG. 8. The leading SVD mode for the DJF (top) precipitation in China and (bottom) the SSTs over the Indian–Pacific Ocean during the winters of 1976–2009. (left) The homogeneous correlation patterns and (right) the heterogeneous correlation patterns. The areas significant at the 0.10 level are colored. The effective degrees of freedom are estimated according to Pyper and Peterman (1998).

differences were calculated for time series of MLYP and the TIOI, and then the linear regression and correlation between them were calculated (Nicholls 2010; Li et al. 2013). The linear regression between year-to-year differences in MLYP and TIOI allow the estimation of the precipitation trend that should be expected from the trend in the TIO through the relationship between MLYP and the TIOI. Accordingly, the sensitivity of MLYP to the TIOI is defined as the slope of the TIOI in the fitted linear regression model for the relationship between year-to-year differences of MLYP and TIOI. Thus, assuming that the relationship derived from the year-to-year differences operates over multidecadal time scales, the MLYP trend induced by the TIO can be estimated from the product of the sensitivity and the trend of the TIOI. Hence, the ratio of the TIO-induced trend value to the observed MLYP trend value (19.89 mm decade^{-1}) measures the contribution of TIOI to the MLYP trend during the period from 1976 to 2009. Similarly, the contributions of other climate modes (EATL/WRUS teleconnection pattern) to the MLYP trend were calculated for comparison (Table 3). We can see from Table 3 that the MLY wetting trends induced by the EATL/WRUS teleconnection pattern and TIOI are 2.85 and 16.46 mm decade^{-1}, respectively. In other words, the warming SST in the TIO can explain 82.7% of the observed increasing trend (19.89 mm decade^{-1}) in MLYP, but the EATL/WRUS teleconnection pattern can only explain 14.3%. Therefore, the warming SST in the TIO has contributed more than 80% of the recent MLYP wetting trend in winter over the period 1976–2009.

6. Dynamical effects of TIO warming on MLY precipitation

To investigate how the TIO warming intensifies precipitation over the MLY in winter, we investigated the dynamical effects of a warmer SST in the TIO on atmospheric circulation over the MLY via diabetic heating.

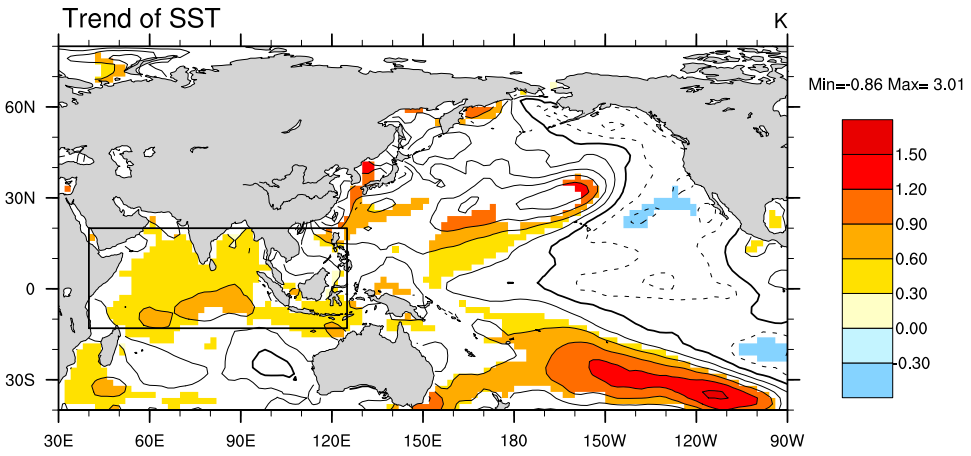

FIG. 9. Linear trends of the winter mean SSTs (K) over the last 34 yr from 1976 to 2009. The contour interval is 0.25 K. The thin black (thin dashed) contours denote positive (negative) values, and bold black contours denote zero. The areas with significant trends at the 0.05 level are colored. The effective sample sizes were reestimated according to Zwiers and von Storch (1995). The rectangular box marks the TIO area (13°S–20°N, 40°–125°E).

a. *Moisture flux over eastern China driven by TIO warming*

Figure 10 shows the correlations between the TIOI and SLP and horizontal moisture vectors in the lower troposphere. The zonal and meridional moisture flux components are respectively defined as uq and vq, where q is relative humidity, u is the zonal wind component, and v is the meridional wind component. The remarkable feature is the occurrence of the significant cyclonic southerly correlation of vectors between the TIOI and horizontal moisture vectors, which is very similar to the anomalous cyclonic circulations associated with the positive MLYP shown in Fig. 6a. This similarity suggests that the anomalous cyclonic southerly (anticyclonic northerly) associated with the MLYP variability (as shown in Fig. 6a) is mainly associated with, or caused by, the warmer (cooler) TIO. In particular, a significantly negative correlation occurs between the TIOI and SLP over the MLY, indicating that the anomalous cyclonic southerly (anticyclonic northerly) moisture flux driven by a warmer (cooler) TIO shifts from an anomalous southeast (northwest) wind to a southwest (northeast) wind over the MLY, causes anomalous moisture convergence (divergence) over the MLY, and results in more (less) precipitation over the MLY. In short, the warmer TIO instigates more MLY precipitation through causing a moisture convergence over the MLY area, which is associated with the cyclonic shift of the anomalous southerly. Given that the TIO is warming in recent decades, as demonstrated in Fig. 9, we can therefore infer the MLY wetting during winters of 1976–2009 is driven by the TIO warming through enhancing the anomalous cyclonic southerly and the moisture convergence over the MLY during the same period.

In addition, significant positive correlations between the TIOI and SLP are observed over much of the northwestern Pacific, and negative correlations between them are observed over much of mainland China (except the Tibetan Plateau), centered on the MLY, as shown in the color contours of Fig. 10. This suggests that the warmer (cooler) TIO causes a pressure increase (decrease) over the northwest Pacific, but a pressure decrease (increase) over mainland China, forming a reduced (enhanced) east–west pressure gradient between the mainland of China and the northwest Pacific. And this kind of pressure gradient tends to induce an anomalous cyclonic southerly

TABLE 3. Sensitivity of winter MLYP associated with the EATL/WRUS pattern index and TIOI, as well as their trends and induced MLYP trends in winter over the period 1976–2009. Sensitivity was estimated by applying the regression (slope) between year-to-year changes (removing the linear trend) in MLYP and the index. The induced MLYP trend is the product of the sensitivity and the index trend for 34 yr (1976–2009). Correlations or regressions significant at the 0.05 level are in bold. The effective sample sizes were re-estimated according to Zwiers and von Storch (1995). The TIOI accounts for 82.7% of the trend in MLYP.

	EATL/WRUS pattern index	TIOI
Correlation (year-to-year differenced data)	0.33	**0.44**
Sensitivity (mm unit^{-1})	19.66	**124.53**
Trend (unit decade^{-1})	0.15	**0.14**
Induced MLYP trend (mm decade^{-1})	2.92	16.85
Contribution (%) to the MLYP trend (20.38 mm decade^{-1})	14.3	82.7

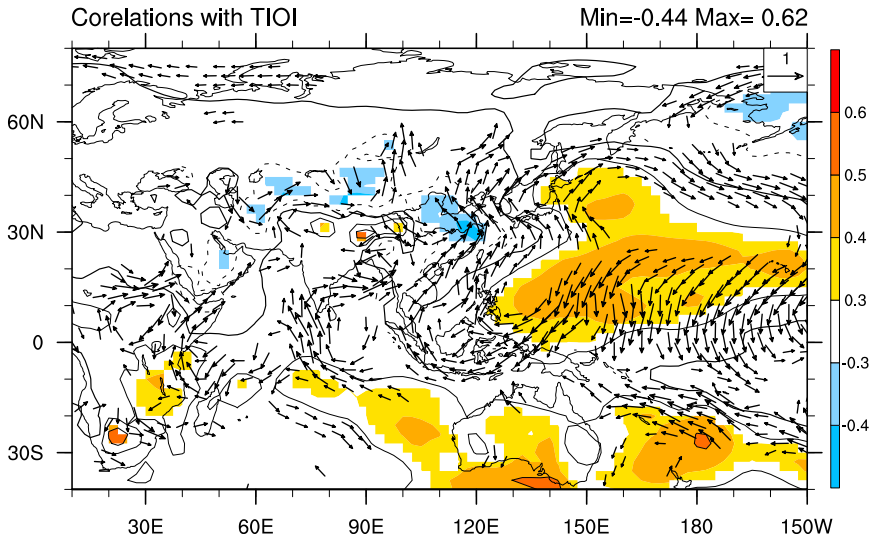

FIG. 10. Correlations of the TIOI with SLP (contours) and horizontal moisture vectors at 850 hPa in the winter during the period 1976–2009. The vectors are of correlations significant above the 0.10 level, the two components of which are the correlation coefficients between the MLYP and anomalously zonal moisture flux, and between the MLYP and anomalously meridional moisture flux. The contour interval is 0.25; thin black (thin dashed) contours denote positive (negative) trends; the bold black contours denote zero. The areas with correlation between the TIOI and SLP significant at the 0.10 level are colored. The effective degrees of freedom were estimated according to Pyper and Peterman (1998).

(anticyclonic northerly) over the coastal area of eastern China and convergence (divergence) over the MLY area. Previous studies have already documented that a warmer Indian Ocean causes an intensification of the pressure in the northwestern Pacific (i.e., the western Pacific subtropical high) during both winter (e.g., Hoerling et al. 2004) and summer seasons (e.g., Wu and Liu 1992; Yang et al. 2007; Xie et al. 2009; T. Zhou et al. 2009), supporting the results of this study. Thus, the result that a warmer (cooler) TIO drives a cyclonic southerly (anticyclonic northerly) along the coastal area of eastern China and convergence (divergence) over the MLY area in winter is reasonable.

In short, a warming TIO can cause precipitation to increase over the MLY by enhancing the moisture convergence over the MLY, which is associated with an anomalous cyclonic southerly along the coast of eastern China. As the anomalous southerly over eastern China in winter indicates the weakening of the EAWM, we can also conclude that a warming TIO causes precipitation increase over the MLY through weakening the monsoonal circulations over the MLY area. More detailed thermal forcing processes of the warmer TIO that causes the precipitation increase over the MLY need further study by numerical simulations.

b. *Modeling atmospheric response to TIO warming*

To further explore and verify the role of TIO warming in driving the recent wintertime wetting trend over the MLY, we conducted SST forcing experiments using a spectral atmospheric model (SAMIL-R42L9). In the control simulation, we imposed the perpetual mean January climate to simplify the experiment and prevent disturbance from other (i.e., not winter) seasons. To achieve this, the solar height angle, length of day, and SST were all set to their mean January values. This method of setting model simulations follows Wu and Liu (1992) and Li et al. (2013). The main features of the winter circulations were reproduced successfully in the control experiment (Wu et al. 2003, 2012). We have conducted both a warmer TIO forcing and a cooler TIO forcing experiment to demonstrate the thermal forcing by TIO SSTs on precipitation variability over the MLY. In these two experiments, we imposed the same perpetual mean January climate, except the reverse thermal forcing in the TIO region (20°S–20°N, 40°–110°E). To make the simulated results more easily comparable with observational results, we used the observed linear trend for winter from 1976 to 2009 over the region as the SST forcing, except their values were doubled, added, or subtracted from the mean January SST in boundary over the above TIO region (Figs. 11a and 12a). Both the control and thermal forcing experiments were integrated up to 60 months, which is equivalent to 60 winters in our scenario. The spin-up time in these experiments was less than 20 winters. We assessed whether the value of the energy budget at the top of the

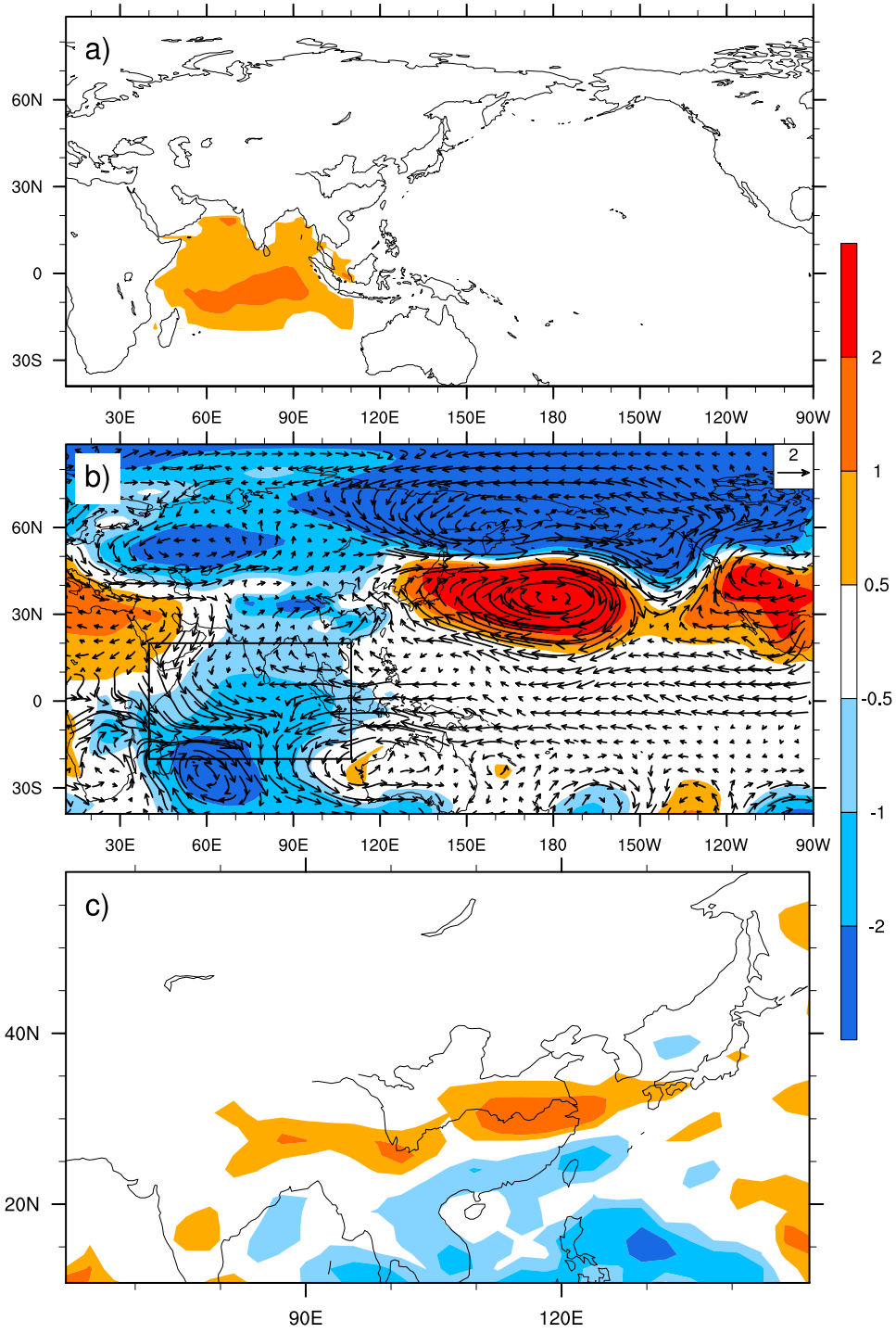

FIG. 11. The difference between the enhanced SST and control simulations of winter (a) SST (K), (b) surface pressure (hPa) and 850-hPa wind vectors (m s^{-1}), and (c) precipitation (mm day^{-1}). Black box in (b) denotes the location of SST forcing in (a).

atmosphere reached its quasi-asymptotic value and used this as a criterion to judge if the model had integrated to the equilibrated state. This method follows Simmonds (1985). Differences between the enhanced (decreased) SST and control experiments were then computed from data covering the last 30 winters to show the thermal forcing effects of TIO SST.

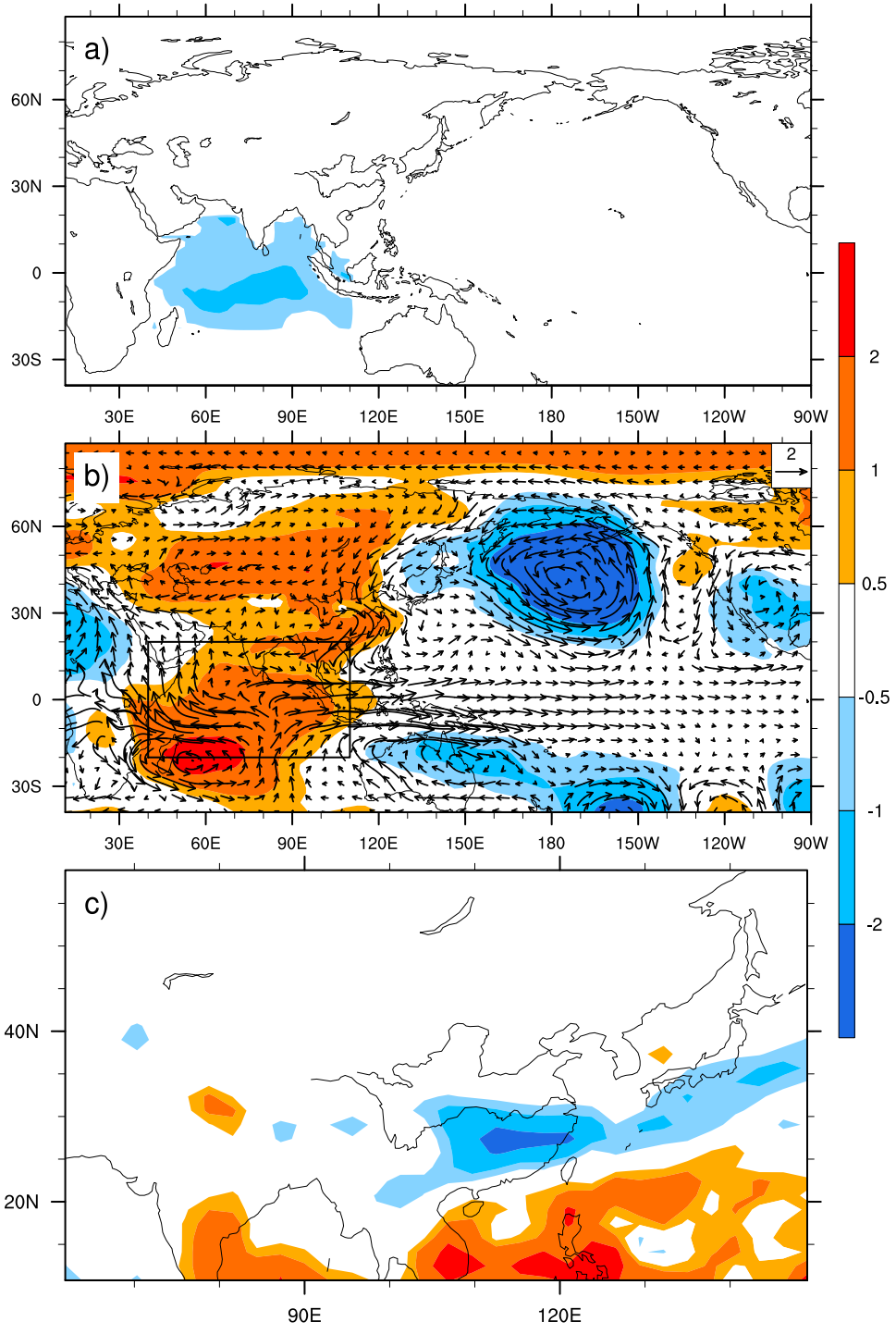

FIG. 12. As for Fig. 11, but for the cooling TIO SST forcing experiment.

Figure 11 shows that the increased precipitation over the MLY driven by the warm SST in the TIO is well simulated by the warmer TIO forcing experiment. The warmer SST forcing over the TIO is shown in Fig. 11a. And the anomalously cyclonic southerly along the coastal area of eastern China is exhibited as a robust response of the tropospheric circulation over the MLY to the warmer SST in the TIO, as shown in Fig. 11b. And such an anomalous cyclonic southerly over the MLY causes a moisture convergence over the MLY. As a

response to the moisture convergence over the MLY, the precipitation over the MLY is increased, as shown in Fig. 11c. So, the simulated results are very similar to the observations (cf. Figs. 11b and 10 and Figs. 11c and 1), which demonstrates that the diabetic warming over the TIO can intensify the precipitation over the MLY.

In particular, the south and north parts of the cyclonic southerly along the coast of eastern China (Fig. 11b), or the southwesterly over southeastern China and the southeasterly over northeastern China, are both responses to TIO thermal forcing, but they seem not to respond in the same way. As to the south part of the anomalous cyclonic southerly, the anomalous southwesterly over southeastern China, we explain it mainly as a direct Gill-type response to the warmer TIO. This anomalous southwesterly is extended out anticyclonically from the northeast corner of the warmer TIO region (as marked by the rectangle in Fig. 11), which is one of the classic Gill-type responses to the diabetic heating as a result of the eastward propagation of Kelvin waves, according to the early study of Gill (1980). Other direct Gill-type responses of tropospheric circulations to the diabetic heating of the warmer TIO can also be observed in Fig. 11b, including the anomalous anticyclone that occurs in the southeast corner of the TIO because of the eastward propagation of Kelvin waves and a pair of anomalous cyclonic circulations that occur in the northwest and southwest corners of the TIO because of the westward propagation of Rossby waves. As to the north part of the anomalous cyclonic southerly, the anomalous southeasterly over northeastern China, however, we can hardly explain it as a Gill-type response to the warmer TIO because of two difficulties. One difficulty is the anomalous cyclonic wind direction over the MLY is the opposite of the expected wind direction (anticyclonic) of the Gill-type response in this area, and the other difficulty is the location of the anomalous southeasterly (over northeastern China) is a little far away from the location of the TIO thermal forcing area. We therefore explain the anomalous southeasterly over northeastern China mainly as part of the positive North Pacific Oscillation (NPO)-like pattern over the northern Pacific responding to the warmer TIO forcing. The southern action center of the positive NPO-like pattern, an anticyclone structure (as shown in Fig. 11b), reaches northern China, drives the anomalous southeasterly over the coastal area of northeastern China, and induces a wind shift and moisture convergence over the MLY that results in increased precipitation (as shown in Fig. 11c).

In previous studies, NPO influences on interannual precipitation variability over MLY have been observed (Wang et al. 2011), and a remote NPO-like response in the northern Pacific to the warmer forcing in TIO in winter has already been documented using different numerical models (e.g., Wu and Liu 1992; Hoerling et al. 2004; T. Zhou et al. 2009). Specifically, Xie et al. (2009) have explained a similar remote response of the anomalous anticyclone over the northwest Pacific in summer as a ''capacitor effect'' of the warm tropospheric Kelvin wave that is responding to TIO warming, suggesting that the NPO-like pattern over the northern Pacific seems not to be a direct Gill-type response to thermal forcing of TIO warming. These all support the results of our study.

In addition, the geographic location of the MLY and the shape of the coastline of eastern China may also be necessary elements in generating the cyclonic southerly response under the forcing of TIO warming. Because of the larger fraction of wind over the land area compared with the ocean and the sharp land–sea thermal contrast near coastlines, strong wind flows occur along the coastal area. Meanwhile, the coastal line of eastern China reaches its easternmost point near the MLY, which in turn favors a cyclonic coastal wind shift in this area.

Thus, the diabatic warming over the TIO intensifies the precipitation over the MLY by driving a cyclonic southerly along the coast of eastern China, and the cyclonic southerly over the coast of eastern China is a combination of the Gill-type thermal response near the northeast corner of the TIO region and the remote NPO-like response over the northern Pacific.

A cooler TIO forcing experiment was conducted as a comparison with the above warmer TIO simulation. The cooler SST forcing over the TIO is shown in Fig. 12a and is the complete opposite of the warmer SST forcing in Fig. 11a. The results show reversed atmospheric circulation and decreased precipitation over the MLY, responding to the cooler TIO SST forcing, but the circulation response to the cooler TIO SST forcing shows a little asymmetry compared to the circulation response to the warmer TIO SST forcing. In Fig. 12b, an anomalous intensified Aleutian low response occurs over the northern Pacific, the southwest corner of which reaches north China and drives the anomalous northwesterly over the coast of northeastern China. Meanwhile, an anomalous anticyclonic response occurs over the northwest of the TIO (Fig. 12b) because of the propagation of Kelvin waves responding to the diabetic heating (Gill 1980) of cooler TIO SSTs, which exhibits as the anomalous northeasterly over the coastal area of southeastern China and induces wind shift and moisture divergence over the MLY, resulting in less precipitation (Fig. 12c). Comparing the precipitation response to cooler TIO forcing (Fig. 12c) with that to warmer TIO

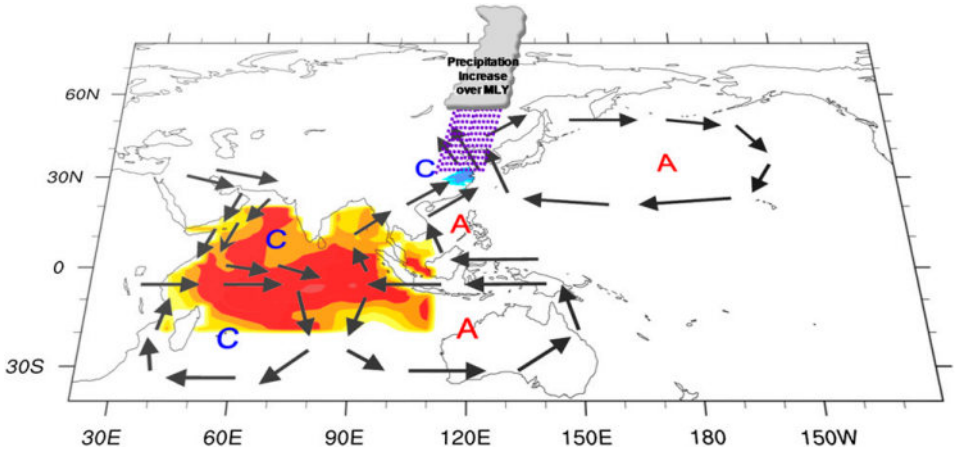

FIG. 13. Schematic representation of the winter precipitation increase in MLY caused by the TIO warming in recent decades. The "A" denotes the anticyclonic circulation and "C" denotes the cyclonic circulation.

forcing (Fig. 11c), we can see that the precipitation anomalies over the MLY are reversed, except that the anomalous negative precipitation belts under the cooler TIO SST forcing are shifted a little southward. Therefore, both the cooler- and warmer TIO SST forcing experiments demonstrated that TIO SST is an important driver of precipitation variability in the MLY in the boreal winter.

Overall, as shown schematically in Fig. 13, thermal forcing instigated by the increasing SST over the TIO gives rise to the anomalous southwesterly over southeastern China mainly through its Gill-type response near the TIO region, and it gives rise to the anomalous southeasterly over northeastern China mainly through the remote response of the positive NPO-like pattern over the northern Pacific, forming the cyclonic southerlies along the coast of eastern China (or the weakening EAWM circulation), causing wind shift and moisture convergence over the MLY, and, consequently, resulting in increased precipitation.

7. Discussion and summary

This study investigated the precipitation trend in MLY over the latest three decades since the late 1970s. We found that a significant wetting trend has dominated the MLY, forming a "mid-east-China winter wetting" pattern over eastern China during the winters between 1976 and 2009. This precipitation increase appears reasonable and coincides well with the weakening of the EAWM circulation.

We investigated the driving mechanism of this wetting trend in MLYP and found that two key factors are closely connected to the variability of wintertime MLY precipitation: the EATL/WRUS pattern, one of the EU patterns documented by Barnston and Livezey (1987) and Liu et al. (2014) that extends from upstream at high latitudes in northern China, and the SST variability over the TIO in tropical regions. Although the EATL/WRUS pattern is closely connected with the MLYP, it cannot be the major driver of the MLY precipitation trend because of its lack of a linear trend over the same period. In contrast, the increasing SST in the TIO plays a predominant role in the precipitation increase in the MLY. That is, the increased SST in the TIO drives an anomalous cyclonic southerly along the coast of eastern China and the anomalous wind shift over the MLY, which brings more moisture to the MLY from the tropical oceans and leads to water vapor convergence over the MLY, resulting in increased precipitation (Fig. 13). Results obtained from numerical experiments also demonstrate that the increased (decreased) tropical SST around the TIO can intensify (reduce) inland precipitation over the MLY by instigating the anomalous cyclonic southerly (anticyclonic northerly) over the MLY. It should be noted that the south part of the anomalous cyclonic southerly (anticyclonic northerly) over the coastal area of eastern China, or the anomalous southwesterly (northeasterly) over southeastern China, is mainly a direct Gill-type response to the warmer (cooler) TIO forcing near the northeast corner of the TIO region; but the north part of the anomalous cyclonic southerly (anticyclonic northerly) over the coastal area of eastern China, or the southeasterly (northwesterly) over northeastern China, is mainly part of the positive NPO-like (enhanced Aleutian low) pattern response to the warmer (cooler) TIO forcing in the remote

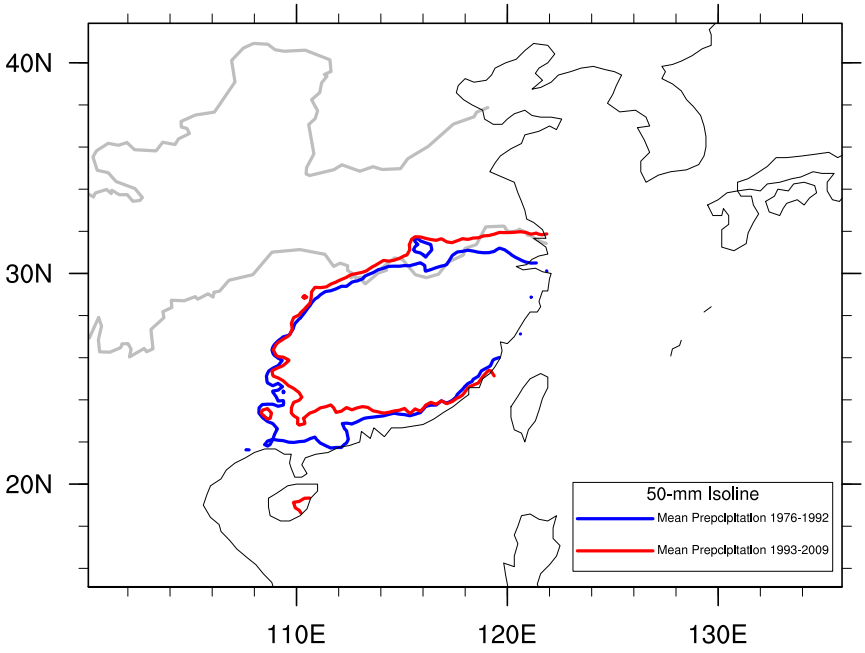

FIG. 14. The shift in winter precipitation climatology over southern China between 1976 and 2009 indicated by the change in the position of the 50-mm isoline between 1976–92 (blue contour) and 1993–2009 (red contour).

northwestern Pacific. Therefore, the increase in winter precipitation over the MLY results from an anomalous cyclonic circulation along the coastal area of eastern China (or the weakening EAWM circulation) responding to the warming SST in the TIO.

As most winter precipitation falls in southern China and the MLY is located on the northern edge of southern China, the fact that the significant wetting trend occurs over the MLY but no significant precipitation trend occurs in other subregions of southern China suggests the northward extension of the precipitation belts in southern China in recent decades. This extension is clearly shown by the climatological precipitation records for the periods 1976–92 and 1993–2009 (Fig. 14). The spatial location of the 50-mm isoline for 1976–92 had shifted northward by about 2° (about 200 km) in latitude by 1993–2009. Thus, the precipitation increase over the MLY indicates the manifestation of the northward extension of precipitation belts in the southern Chinese winter.

This northward extension of the precipitation belt over southern China agrees well with previous studies that suggest the poleward expansion of the global dry zone under the expanding Hadley circulation (Chen et al. 2002; Fu et al. 2006; Lu et al. 2007; Feng et al. 2013). The intensity and spatial scope of the Hadley circulation can be well represented by the zonal mean meridional streamfunction (ZMSF) in the tropics (e.g., Peixoto and Oort 1992; Oort and Yienger 1996; Waliser et al. 1999). As shown in Fig. 15a, the northern branch of the climatological Hadley circulation represented by a positive ZMSF in the tropics is mainly located approximately south of 30°N in the free troposphere and located approximately south of 40°N in the boundary layer in winter. In contrast, the positive ZMSF regressed onto the MLYP (Fig. 15b) expands from the equator to 60°N in the tropics, which is broader than the climatological scope of the northern branch of the Hadley circulation. This implies that the wetting trend over the MLY coincides with the expansion of the Hadley circulation. Besides, the correlation between variability of the MLYP and the location of the north border of the Hadley circulation (LHC) in the Northern Hemisphere suggests the same conclusion. The LHC in the Northern Hemisphere can be defined as the longitude at which the mass streamfunction transfers from positive to negative, or the longitude of the zero line in the subtropics of the Northern Hemisphere. The averaged LHC at 850 and 925 hPa during the winters of 1976–2009 is at 34.3° and 39.6°N, respectively. And the variability of the LHC on both levels contains a significant positive trend, indicating the poleward expansion of HC on lower troposphere. The correlation between the MLYP with LHC on surface of 850 and 925 hPa is respectively 0.33 and 0.45, both significant at the 0.1 level after taking account of the effective degrees of freedom

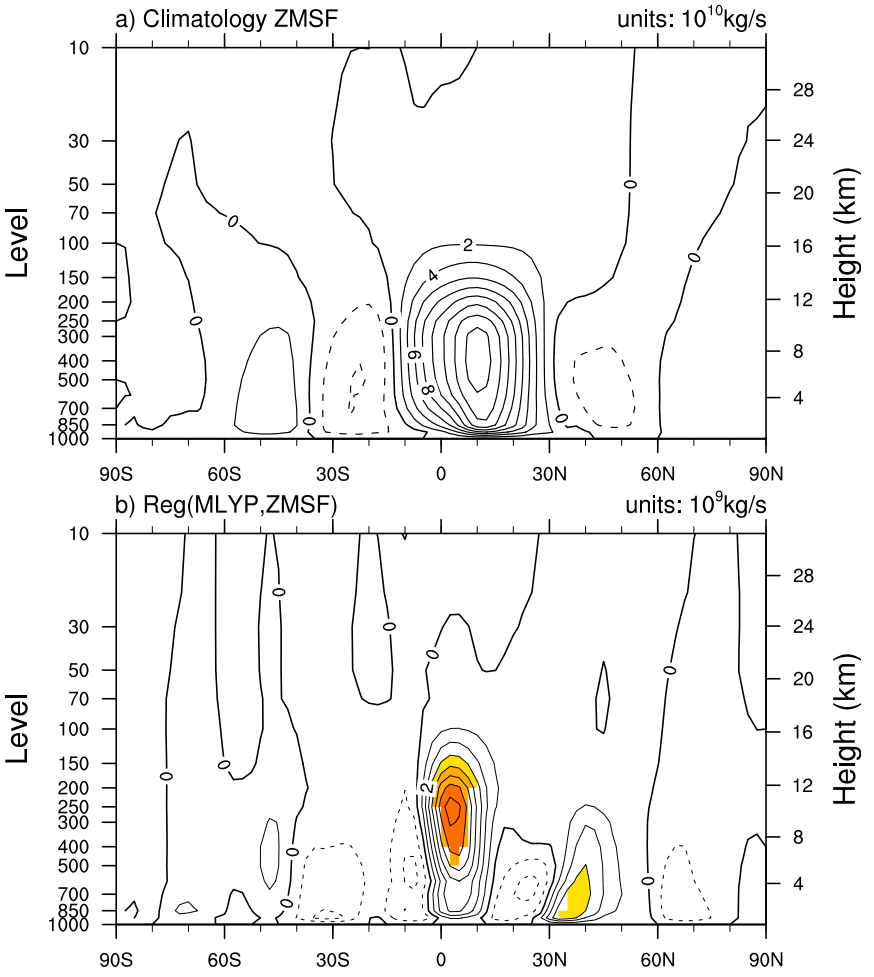

FIG. 15. Map of the regressions (contours, 1 per contour interval; units: $10^9\,\mathrm{kg\,s^{-1}}$) of the global ZMSF onto the normalized MLYP in the winter (DJF) for 1976–2009. The thin black (thin dashed) contours denote positive (negative) values, and bold black contours denote zero. Values above the 0.05 confidence level are color shaded.

(Pyper and Peterman 1998), but respectively drops to 0.22 and 0.29 after trimming their linear trends. This implies that more MLYP occurs when the LHC is located more northerly, and vice versa; but the significant correlations between the MLYP and LHC are mainly contributed by their linear trends. In other words, the MLYP wetting coincides with the poleward expanding of HC. In addition, Ma and Li (2007, 2008) have demonstrated that the TIO is an important driver of the recent enhancement and expansion of the wintertime Hadley circulation, indicating that the MLY wetting is sharing the same SST driver with the Hadley circulation expanding in winter. Therefore, the recent MLY wetting or the extension of precipitation belts of southern China coincides with the poleward expansion of the Hadley circulation.

In summary, the increase in SST in the TIO can be considered as the main driver of the long-term wetting trend in the MLY during the last three decades (1976–2009). The dominant wetting trend in the MLY after 1976 suggests that drought and wet conditions over the MLY show multidecadal variations. Of note, although the EATL/WRUS teleconnection pattern in high latitudes has not played a major role in driving recent wetting over the MLY, this does not mean that factors from high latitudes will not be important for future long-term variations in MLYP. This raises some interesting questions; for example, how do high-latitude factors drive the long-term change in precipitation over the MLY? How will MLY precipitation change in the future? Further work is required to address these questions and to explore the underlying mechanisms.

Acknowledgments. We thank three anonymous reviewers, Prof. Tianjun Zhou, Dr. Jie Song, and Dr. Pengfei Wang, whose comments helped greatly

improve an early version of the manuscript. This research is supported in part by the National Basic Research Program of China (Grant 2010CB950400) and the National Natural Science Foundation of China (Grants 91437216 and 40905040). Yun Li was supported by the CSIRO–Chinese Academy of Sciences Exchange Scheme 2012 and 2014.

REFERENCES

Alory, G., S. Wijffels, and G. Meyers, 2007: Observed temperature trends in the Indian Ocean over 1960–1999 and associated mechanisms. *Geophys. Res. Lett.,* **34,** L02606, doi:10.1029/2006GL028044.

Barnett, T. P., D. W. Pierce, K. M. AchutaRao, P. J. Gleckler, B. D. Santer, J. M. Gregory, and W. M. Washington, 2005: Penetration of human-induced warming into the world's oceans. *Science,* **309,** 284–287, doi:10.1126/science.1112418.

Barnston, A. G., and R. E. Livezey, 1987: Classification, seasonality and persistence of low-frequency atmospheric circulation patterns. *Mon. Wea. Rev.,* **115,** 1083–1126, doi:10.1175/1520-0493(1987)115<1083:CSAPOL>2.0.CO;2.

Bartlett, M., 1935: Some aspects of the time-correlation problem in regard to tests of significance. *J. Roy. Stat. Soc.,* **98,** 536–543.

Bourke, W., 1974: A multi-level spectral model. I. Formulation and hemispheric integrations. *Mon. Wea. Rev.,* **102,** 687–701, doi:10.1175/1520-0493(1974)102<0687:AMLSMI>2.0.CO;2.

Chang, C. P., 2004: *East Asian Monsoon.* Vol. 2. World Scientific Publishing, 564 pp.

——, J. E. Erickson, and K. M. Lau, 1979: Northeasterly cold surges and near-equatorial disturbances over the Winter MONEX area during December 1974. Part I: Synoptic aspects. *Mon. Wea. Rev.,* **107,** 812–829, doi:10.1175/1520-0493(1979)107<0812:NCSANE>2.0.CO;2.

Chen, J., B. E. Carlson, and A. D. Del Genio, 2002: Evidence for strengthening of the tropical general circulation in the 1990s. *Science,* **295,** 838–841, doi:10.1126/science.1065835.

Chen, W., S. Yang, and R.-H. Huang, 2005: Relationship between stationary planetary wave activity and the East Asian winter monsoon. *J. Geophys. Res.,* **110,** D14110, doi:10.1029/2004JD005669.

Deser, C., and A. S. Phillips, 2006: Simulation of the 1976/77 climate transition over the North Pacific: Sensitivity to tropical forcing. *J. Climate,* **19,** 6170–6180, doi:10.1175/JCLI3963.1.

Ding, Y., and T. N. Krishnamurti, 1987: Heat budget of the Siberian high and the winter monsoon. *Mon. Wea. Rev.,* **115,** 2428–2449, doi:10.1175/1520-0493(1987)115<2428:HBOTSH>2.0.CO;2.

Feng, J., J. Li, and F. Xie, 2013: Long-term variation of the principal mode of boreal spring Hadley circulation linked to SST over the Indo-Pacific warm pool. *J. Climate,* **26,** 532–544, doi:10.1175/JCLI-D-12-00066.1.

Fu, Q., C. M. Johanson, J. M. Wallace, and T. Reichler, 2006: Enhanced mid-latitude tropospheric warming in satellite measurements. *Science,* **312,** 1179, doi:10.1126/science.1125566.

Gemmer, M., S. Becker, and T. Jiang, 2004: Observed monthly precipitation trends in China 1951–2002. *Theor. Appl. Climatol.,* **77,** 39–45, doi:10.1007/s00704-003-0018-3.

Gill, A. E., 1980: Some simple solutions for heat-induced tropical circulation. *Quart. J. Roy. Meteor. Soc.,* **106,** 447–462, doi:10.1002/qj.49710644905.

Gong, D. Y., and C. H. Ho, 2002: Shift in the summer rainfall over the Yangtze River valley in the late 1970s. *Geophys. Res. Lett.,* **29,** 1436, doi:10.1029/2001GL014523.

Ho, C. H., J. Y. Lee, M. H. Ahn, and H. S. Lee, 2003: A sudden change in summer rainfall characteristics in Korea during the late 1970s. *Int. J. Climatol.,* **23,** 117–128, doi:10.1002/joc.864.

Hoerling, M. P., J. W. Hurrell, and T. Xu, 2001: Tropical origins for recent North Atlantic climate change. *Science,* **292,** 90–92, doi:10.1126/science.1058582.

——, ——, ——, G. T. Bates, and A. Phillips, 2004: Twentieth century North Atlantic climate change. Part II: Understanding the effect of Indian Ocean warming. *Climate Dyn.,* **23,** 391–405, doi:10.1007/s00382-004-0433-x.

Huang, R., J. Chen, and G. Huang, 2007: Characteristics and variations of the East Asian monsoon system and its impact on climate disasters in China. *Adv. Atmos. Sci.,* **24,** 993–1023, doi:10.1007/s00376-007-0993-x.

Hung, C.-w., and P.-k. Kao, 2010: Weakening of the winter monsoon and abrupt increase of winter rainfalls over northern Taiwan and southern China in the early 1980s. *J. Climate,* **23,** 2357–2367, doi:10.1175/2009JCLI3182.1.

IPCC, 2013: Summary for policymakers. *Climate Change 2013: The Physical Science Basis,* T. F. Stocker et al., Eds., Cambridge University Press, 1–29.

Kumar, K. K., B. Rajagopalan, and M. A. Cane, 1999: On the weakening relationship between the Indian monsoon and ENSO. *Science,* **284,** 2156–2159, doi:10.1126/science.284.5423.2156.

Lee, S. S., S. H. Kim, J. G. Jhun, K. J. Ha, and Y. W. Seo, 2013: Robust warming over East Asia during the boreal winter monsoon and its possible causes. *Environ. Res. Lett.,* **8,** 034001, doi:10.1088/1748-9326/8/3/034001.

Levitus, S., J. Antonov, and T. Boyer, 2005: Warming of the world ocean, 1955–2003. *Geophys. Res. Lett.,* **32,** L02604, doi:10.1029/2004GL021592.

Li, J., and Z. Wu, 2012: Importance of autumn Arctic sea ice to northern winter snowfall. *Proc. Natl. Acad. Sci. USA,* **109,** E1898, doi:10.1073/pnas.1205075109.

Li, X.-F., J. Yu, and Y. Li, 2013: Recent summer rainfall increase and surface cooling over northern Australia since the late 1970s: A response to warming in the tropical western Pacific. *J. Climate,* **26,** 7221–7239, doi:10.1175/JCLI-D-12-00786.1.

Li, Y., J. Li, and J. Feng, 2012: A teleconnection between the reduction of rainfall in southwest Western Australia and north China. *J. Climate,* **25,** 8444–8461, doi:10.1175/JCLI-D-11-00613.1.

Liao, R.-W., Y. Sheng, and D.-B. Zhang, 2013: Characteristics of winter rainfall in eastern China based on grid data. *J. Meteor. Environ.,* **29,** 55–62.

Liu, Y., L. Wang, W. Zhou, and W. Chen, 2014: Three Eurasian teleconnection patterns: Spatial structures, temporal variability, and associated winter climate anomalies. *Climate Dyn.,* **42,** 2817–2839, doi:10.1007/s00382-014-2163-z.

Lu, J., G. A. Vecchi, and T. Reichler, 2007: Expansion of the Hadley cell under global warming. *Geophys. Res. Lett.,* **34,** L06805, doi:10.1029/2006GL028443.

Ma, J., and J. Li, 2007: Strengthening of the boreal winter Hadley circulation and its connection with ENSO. *Prog. Nat. Sci.,* **17,** 1327–1333.

——, and ——, 2008: The principal modes of variability of the boreal winter Hadley cell. *Geophys. Res. Lett.,* **35,** L01808, doi:10.1029/2007GL031883.

Mantua, N. J., S. R. Hare, Y. Zhang, J. M. Wallace, and R. C. Francis, 1997: A Pacific interdecadal climate oscillation with impacts on salmon production. *Bull. Amer. Meteor. Soc.,* **78,** 1069–1080, doi:10.1175/1520-0477(1997)078<1069:APICOW>2.0.CO;2.

Nakamura, H., T. Izumi, and T. Sampe, 2002: Interannual and decadal modulations recently observed in the Pacific storm track activity and East Asian winter monsoon. *J. Climate,* **15,** 1855–1874, doi:10.1175/1520-0442(2002)015<1855:IADMRO>2.0.CO;2.

Nicholls, N., 2010: Local and remote causes of the southern Australian autumn-winter rainfall decline, 1958–2007. *Climate Dyn.,* **34,** 835–845, doi:10.1007/s00382-009-0527-6.

Nitta, T., and S. Yamada, 1989: Recent warming of tropical sea surface temperature and its relationship to the Northern Hemisphere circulation. *J. Meteor. Soc. Japan,* **67,** 375–383.

Oort, A. H., and J. J. Yienger, 1996: Observed interannual variability in the Hadley circulation and its connection to ENSO. *J. Climate,* **9,** 2751–2767, doi:10.1175/1520-0442(1996)009<2751:OIVITH>2.0.CO;2.

Peixoto, J. P., and A. H. Oort, 1992: *Physics of Climate.* American Institute of Physics, 520 pp.

Pyper, B. J., and R. M. Peterman, 1998: Comparison of methods to account for autocorrelation in correlation analyses of fish data. *Can. J. Fish. Aquat. Sci.,* **55,** 2127–2140, doi:10.1139/f98-104.

Rao, S. A., A. R. Dhakate, S. K. Saha, S. Mahapatra, H. S. Chaudhari, S. Pokhrel, and S. K. Sahu, 2012: Why is Indian Ocean warming consistently? *Climatic Change,* **110,** 709–719, doi:10.1007/s10584-011-0121-x.

Shen, Y., M. Feng, H. Zhang, and F. Zhang, 2010: Interpolation methods of China Daily precipitation data (in Chinese). *J. Appl. Meteor. Sci.,* **21,** 279–286.

Shuai, J.-b., P. Guo, and Z. Pang, 2010: Interdecadal variation of the relationship between AO and winter precipitation in China (in Chinese). *Plateau Meteor.,* **29,** 1126–1136.

Simmonds, I., 1985: Analysis of the ''Spinup'' of a general circulation model. *J. Geophys. Res.,* **90,** 5637–5660, doi:10.1029/JD090iD03p05637.

Smith, T. M., R. W. Reynolds, T. C. Peterson, and J. Lawrimore, 2008: Improvements to NOAA's historical merged land–ocean surface temperature analysis (1880–2006). *J. Climate,* **21,** 2283–2296, doi:10.1175/2007JCLI2100.1.

Trenberth, K. E., 1990: Recent observed interdecadal climate changes in the Northern Hemisphere. *Bull. Amer. Meteor. Soc.,* **71,** 988–993, doi:10.1175/1520-0477(1990)071<0988:ROICCI>2.0.CO;2.

——, and J. W. Hurrell, 1994: Decadal atmosphere–ocean variations in the Pacific. *Climate Dyn.,* **9,** 303–319, doi:10.1007/BF00204745.

Waliser, D. E., Z. Shi, J. R. Lanzante, and A. H. Oort, 1999: The Hadley circulation: Assessing NCEP/NCAR reanalysis and sparse in-situ estimates. *Climate Dyn.,* **15,** 719–735, doi:10.1007/s003820050312.

Wallace, J. M., and D. S. Gutzler, 1981: Teleconnections in the geopotential height field during the Northern Hemisphere winter. *Mon. Wea. Rev.,* **109,** 784–812, doi:10.1175/1520-0493(1981)109<0784:TITGHF>2.0.CO;2.

Wang, L., and W. Chen, 2010: How well do existing indices measure the strength of the East Asian winter monsoon? *Adv. Atmos. Sci.,* **27,** 855–870, doi:10.1007/s00376-009-9094-3.

——, and J. Feng, 2011: Two major modes of the wintertime precipitation over China. *Chin. J. Atmos. Sci.,* **35,** 1105–1116.

——, and W. Chen, 2014: An intensity index for the East Asian winter monsoon. *J. Climate,* **27,** 2361–2374, doi:10.1175/JCLI-D-13-00086.1.

——, R. Huang, L. Gu, W. Chen, and L. Kang, 2009: Interdecadal variations of the East Asian winter monsoon and their association with quasi-stationary planetary wave activity. *J. Climate,* **22,** 4860–4872, doi:10.1175/2009JCLI2973.1.

——, W. Chen, S. K. Fong, and K. C. Leong, 2011: The seasonal march of the North Pacific Oscillation and its association with the interannual variations of China's climate in boreal winter and spring. *Chin. J. Atmos. Sci.,* **35,** 393–402, doi:10.3878/j.issn.1006-9895.2011.03.01.

Webster, P. J., A. M. Moore, J. P. Loschnigg, and R. R. Leben, 1999: Coupled ocean–atmosphere dynamics in the Indian Ocean during 1997–98. *Nature,* **401,** 356–360, doi:10.1038/43848.

Wu, G., and H. Liu, 1992: Atmospheric precipitation in response to equatorial and tropical sea surface temperature anomalies. *J. Atmos. Sci.,* **49,** 2236–2255, doi:10.1175/1520-0469(1992)049<2236:APIRTE>2.0.CO;2.

——, and Coauthors, 1997: Global ocean–atmosphere–land system model of LASG (GOALS/LASG) and its performance in simulation study. *Quart. J. Appl. Meteor,* **8,** 15–28.

——, and Coauthors, 2007: The influence of mechanical and thermal forcing by the Tibetan Plateau on Asian climate. *J. Hydrometeor.,* **8,** 770–789, doi:10.1175/JHM609.1.

——, Y. Liu, B. He, Q. Bao, A. Duan, and F.-F. Jin, 2012: Thermal controls on the Asian summer monsoon. *Sci. Rep.,* **2,** 404, doi:10.1038/srep00404.

Wu, T., P. Liu, Z. Wang, Y. Liu, R. Yu, and G. Wu, 2003: The performance of atmospheric component model R42L9 of GOALS/LASG. *Adv. Atmos. Sci.,* **20,** 726–742, doi:10.1007/BF02915398.

Wu, Z., J. Li, B. Wang, and X. Liu, 2009: Can the Southern Hemisphere annular mode affect China winter monsoon? *J. Geophys. Res.,* **114,** D11107, doi:10.1029/2008JD011501.

——, ——, Z. Jiang, and J. He, 2011: Predictable climate dynamics of abnormal East Asian winter monsoon: Once-in-a-century snowstorms in 2007/2008 winter. *Climate Dyn.,* **37,** 1661–1669, doi:10.1007/s00382-010-0938-4.

Xie, S.-P., K. Hu, J. Hafner, H. Tokinaga, Y. Du, G. Huang, and T. Sampe, 2009: Indian Ocean capacitor effect on Indo–Western Pacific climate during the summer following El Niño. *J. Climate,* **22,** 730–747, doi:10.1175/2008JCLI2544.1.

Xu, M., C. P. Chang, C. Fu, Y. Qi, A. Robock, D. Robinson, and H. Zhang, 2006: Steady decline of east Asian monsoon winds, 1969–2000: Evidence from direct ground measurements of wind speed. *J. Geophys. Res.,* **111,** D24111, doi:10.1029/2006JD007337.

Yang, J., Q. Liu, S.-P. Xie, Z. Liu, and L. Wu, 2007: Impact of the Indian Ocean SST basin mode on the Asian summer monsoon. *Geophys. Res. Lett.,* **34,** L02708, doi:10.1029/2006GL028571.

Zhai, P., and X. Pan, 2003: Change in extreme temperature and precipitation over northern China during the second half of the 20th century. *Acta Geogr. Sin.,* **58,** 1–10.

——, X. Zhang, H. Wan, and X. Pan, 2005: Trends in total precipitation and frequency of daily precipitation extremes over China. *J. Climate,* **18,** 1096–1108, doi:10.1175/JCLI-3318.1.

Zhang, H., J. Qin, and Y. Li, 2011: Climatic background of cold and wet winter in southern China: Part I observational analysis. *Climate Dyn.,* **37,** 2335–2354, doi:10.1007/s00382-011-1022-4.

Zhang, L., X. Zhu, K. Fraedrich, F. Sielmann, and X. Zhi, 2014: Interdecadal variability of winter precipitation in Southeast China. *Climate Dyn.,* **43,** 2239–2248, doi:10.1007/s00382-014-2048-1.

Zhang, Y., K. R. Sperber, and J. S. Boyle, 1997a: Climatology and interannual variation of the East Asian winter monsoon: Results from the 1979–95 NCEP/NCAR reanalysis. *Mon. Wea. Rev.,* **125,** 2605–2619, doi:10.1175/1520-0493(1997)125<2605:CAIVOT>2.0.CO;2.

——, J. M. Wallace, and D. S. Battisti, 1997b: ENSO-like interdecadal variability: 1900–93. *J. Climate,* **10,** 1004–1020, doi:10.1175/1520-0442(1997)010<1004:ELIV>2.0.CO;2.

Zhou, B., and Coauthors, 2011: The great 2008 Chinese ice storm: Its socioeconomic–ecological impact and sustainability lessons learned. *Bull. Amer. Meteor. Soc.,* **92,** 47–60, doi:10.1175/2010BAMS2857.1.

Zhou, L.-T., 2011: Impact of East Asian winter monsoon on rainfall over southeastern China and its dynamical process. *Int. J. Climatol.,* **31,** 677–686, doi:10.1002/joc.2101.

——, and R. Wu, 2010: Respective impacts of the East Asian winter monsoon and ENSO on winter rainfall in China. *J. Geophys. Res.,* **115,** D02107, doi:10.1029/2009JD012502.

Zhou, T., and Coauthors, 2009: Why the western Pacific subtropical high has extended westward since the late 1970s. *J. Climate,* **22,** 2199–2215, doi:10.1175/2008JCLI2527.1.

Zhou, W., J. C. L. Chan, W. Chen, J. Ling, J. G. Pinto, and Y. Shao, 2009: Synoptic-scale controls of persistent low temperature and icy weather over Southern China in January 2008. *Mon. Wea. Rev.,* **137,** 3978–3991, doi:10.1175/2009MWR2952.1.

Zwiers, F. W., and H. von Storch, 1995: Taking serial correlation into account in tests of the mean. *J. Climate,* **8,** 336–351, doi:10.1175/1520-0442(1995)008<0336:TSCIAI>2.0.CO;2.